UNIVERSITY OF TURKU

EXPLORING CONNECTIONS BETWEEN OPEN QUANTUM SYSTEMS, RELATIVITY AND COMPLEX QUANTUM NETWORKS

Boris Sokolov

TURUN YLIOPISTON JULKAISUJA – ANNALES UNIVERSITATIS TURKUENSIS
SARJA – SER. AI OSA – TOM. 632 | ASTRONOMICA – CHEMICA – PHYSICA – MATHEMATICA | TURKU 2020

UNIVERSITY OF TURKU

EXPLORING CONNECTIONS BETWEEN OPEN QUANTUM SYSTEMS, RELATIVITY AND COMPLEX QUANTUM NETWORKS

Boris Sokolov

TURUN YLIOPISTON JULKAISUJA – ANNALES UNIVERSITATIS TURKUENSIS
SARJA – SER. AI OSA – TOM. 632 | ASTRONOMICA – CHEMICA – PHYSICA – MATHEMATICA | TURKU 2020

University of Turku

Faculty of Science and Engineering
Department of Physics and Astronomy
Laboratory of Theoretical Physics
Doctoral Programme in Physical and Chemical Sciences

Supervised by

Iiro Vilja
Department of Physics and Astronomy
University of Turku
Finland

Sabrina Maniscalco
Department of Physics and Astronomy
University of Turku
Finland

Reviewed by

Dr. Inés de Vega
Arnold Sommerfeld Center for Theoretical Physics
Ludwig-Maximilians University of Munich
Germany

Prof. Sergey Filippov
Department of Theoretical Physics
Moscow Institute of Physics and Technology
Russian Federation

Opponent

Dr. Maria Luisa Chiofalo
Physics Department
University of Pisa
Italy

ISBN 978-951-29-8235-6 (PRINT)
ISBN 978-951-29-8236-3 (PDF)
ISSN 0082-7002 (Print)
ISSN 2343-3175 (Online)
Painosalama Oy, Turku, Finland 2020

Acknowledgements

And so it is finally finished, the biggest project of my life so far. It has brought along many adventures, both expected and unexpected, but most of them fun and memorable. It has taught me new skills, practical and impractical, taught me new things about myself and about the surrounding world. And it has introduced me to many fine people, some of whom became my very dear friends. Overall I am quite satisfied of how it turned out.

The project would not have been possible without my supervisors Dr. Iiro Vilja, who has been one of my favorite lecturers since the first year of bachelor studies and whose competence in multiple fields is astounding, and Prof. Sabrina Maniscalco, who has always used her expertise in the most outlandish and wonderful scientific ideas and projects and whom I am very happy to consider one of the aforementioned dear friends of mine. To them I would like to extend my deepest gratitude, they have been my expert guiding hand through all these PhD years and before. Their skill and knowledge have been fundamental to the success of this project.

I also wish to thank the pre-examiners of this thesis, Dr. Inès de Vega and Prof. Sergey Filippov, their reviews were educational and provided insight into making the thesis a more rigorous and pedagogical work.

On the practical side, I very much appreciate the financial support of the Jenny and Antti Wihuri foundation, the Finnish Cultural Foundation, the Väisälä fund, the Turku University Foundation, and the PCS graduate school.

My family, especially my mother Ludmila, and my aunt Irina as well as the light of my life, Julia, deserve my fullest appreciation. They have been an endless source of encouragement and support.

I cannot leave unmentioned my closest collaborators Matteo with his impeccable coding skills and Guille with his amazing solution finding ability. Not forgetting the other, current and former TQT members: Francesco, Johannes, Henri, Mikko, Sina, Leevi, Oskari, Juho, Walter, Nicola, Laura, Tom, Jose, Riku, Daria, Jaakko, Peter, Dario, Erkka, Cate and Rebecca,

having you as friends and co-workers has been a pleasure. Special thanks go to my out-of-work friends Mikko (same one), Ville, Kirsi and my most long-term friends Gleb and Victor.

At last, I would like to thank Wikipedia for inspiring me to apply for a physics degree in the first place.

.. thanks!

Contents

Abstract

This thesis is a collection of works focusing on interrelations between the fields of special relativity, open quantum systems and complex networks. As each of the aforementioned fields encompasses a huge variety of topics, the thesis contains a selection of particular connections.

The first half of the thesis considers an open quantum systems approach to the description of relativistic phenomena. As the aforementioned phenomena often involve dynamically evolving counterparts, some non-Markovian aspects of open quantum systems are initially explored. Conditions for complete positivity are derived for a type of phase-covariant time-local master equation and then applied to a non-Markovian master equation with heuristically-derived decay rates. This is relevant in cases when the physicality of the master equation cannot be postulated.

The first relativistic system considered is a superposition of coherent states in a gravitational gradient. It is shown to exhibit decoherence induced by gravitational time dilation through interaction between inner degrees of freedom and the centre of mass of the superposition. The decoherence is quantified using various, widely-used non-classicality measures. The decoherence rates are then compared to decoherence induced by classical noise to roughly evaluate the experimental precision necessary to detect gravitationally induced decoherence.

In the second relativistic system, the Unruh effect is modeled as an open system where an Unruh-deWitt detector is interacting with bosonic fields. A master equation with time-dependent decay rates for the open system is derived by assuming a non-conventional spacetime path profile for the detector. A particular parameter governing the physical evolution is identified. The system is shown to exhibit non-Markovianity within the completely positive domain of the master equation, the latter ensured by the conditions derived before.

The second half of the thesis starts with a definition of complex networks, which are yet not a commonly used tool in quantum physics. The

concept of pairwise tomography networks is then introduced as a way to represent many-body quantum states.

As the number of pairwise connections grows quadratically with the number of nodes, an efficiently scaling measurement scheme to recover the pairwise tomography networks is presented. The scheme and the concept of pairwise tomography networks are demonstrated to be useful in various applications and the results of a proof-of-principle experiment are shown.

One application explored is a paradigmatic spin chain model known as the XX model. A pairwise entanglement network representation of the XX model is shown to suggest new phenomena such as gradual establishment of quasi-long range order accompanied by a symmetry regarding single-spin concurrence distributions. The existence of structural classes and a cyclic self-similarity in the state are revealed.

Tiivistelmä

Tämä väitöskirja on erikoisen suhteellisuusteorian, avoimien kvanttisysteemien ja kompleksisten verkkojen alojen läpileikkauksiin keskittyvä kokoelma. Sillä jokainen edellämainituista aloista sisältää valtavan moninaisuuden erilaisia käsitteitä, väitöskirjaan sisältyy valikoima tietynlaisia yhteyksiä.

Väitöskirjan ensimmäinen puolisko käsittelee avoimien kvanttisysteemien lähestymistapaa relativististen ilmiöiden kuvaamiseen. Edellä mainitut ilmiöt yleensä sisältävät dynaamisesti kehittyviä osia, joten tutkitaan avoimien kvanttisysteemien ei-markovisia näkökulmia. Täyspositiivisuuden ehdot johdetaan tietyntyyppiselle faasi-kovariantille ajassa lokaalille master-yhtälölle. Nämä ehdot sovitellaan ei-markoviselle master-yhtälölle jossa on heuristisesti johdetut hajoamisnopeudet. Tämä on merkityksellistä silloin kun master-yhtälön fysikaalisuus ei ole postuloitavissa.

Ensimmäinen tarkasteltu relativistinen systeemi on koherenttien tilojen superpositio gravitationaalisessa gradientissa. Sen osoitetaan ilmentävän gravitaationaalisen aikadilataation aiheuttamaa dekoherenssiä sisäisten vapausasteiden ja massakeskipisteen välisten vuorovaikutusten kautta. Tämä dekoherenssi kvantifioidaan käyttämällä useilla laajassa käytössä olevilla ei-klassisuusmitoilla. Dekoherenssinopeuksia verrataan klassisen melun aiheuttamaan dekoherenssiin alustavan gravitaation indusoiman dekoherenssin kokeelliseen havaintoon tarvittavan mittaustarkkuusarvion tekemiseksi.

Toisessa tarkasteltavassa relativistisessa systeemissä, Unruhin ilmiö mallinnetaan avoimena kvanttisysteeminä jossa Unruh-deWitt detektori vuorovaikuttaa bosonikenttien kanssa. Olettamalla detektorille epätavanomainen aika-avaruuspolkuprofiili johdetaan avoimelle kvanttisysteemille master-yhtälö ajasta riippuvin hajoamisnopeuksin. Tunnistetaan erityinen fyysista evoluutiota hallitseva parametri. Systeemin näytetään omaavan ei-markovisuutta master-yhtälön täyspositiivisilla alueilla, täyspositiivisuus taataan aiemmin johdetulla tavalla.

Väitöskirjan toisen puoliskon alussa määritellään kompleksiset kvantti-

verkot, jotka eivät vielä ole laajasti käytettyjä työkaluja kvanttifysiikassa. Esitellään uusi tapa esittää monikappalekvanttitiloja parittaisina tomografiaverkkoina.

Parittaisten yhteyksien lukumäärän ollessa neliöllisesti verrannollinen solmupisteiden lukumäärään, esitetään tehokkaasti skaalautuva parittaisia tomografiaverkkoja muodostava mittausskeema. Skeema ja parittaisten tomografiaverkkojen konsepti osoitetaan hyödyllisiksi erilaisissa sovelluksissa ja esitetään periaatetodistuskokeen tulokset.

Eräänä sovelluksena esitetään XX mallina tunnettu paradigmaattinen spinketjumalli. XX mallin parittaisen kietoutumisen verkkoesityksen näytetään tuovan ilmi uusia ilmiöitä kuten vaiheittaisen kvasipitkän etäisyyden järjestyksen yksittäisten spinien konkurrenssidistribuutioiden symmetrialla. Paljastetaan tilan rakenteellisten luokkien ja syklisten itse-samankaltaisuuksien olemassaolo.

List of papers

This thesis consists of a review of the subject and the following original research articles:

I **Complete positivity, finite temperature effects, and additivity of noise for time-local qubit dynamics**,
J. Lankinen, H. Lyyra, *B. Sokolov*, J. Teittinen, B. Ziaei, S. Maniscalco, Phys. Rev. A **93**, 052103 (2016); Erratum Phys. Rev. A **94**, 059904 (2016)

II **Quantum to classical transition induced by gravitational time dilation**,
B. Sokolov, I. Vilja, S. Maniscalco, Phys. Rev. A **96**, 012126 (2017)

III **Unruh effect and information flow**,
B. Sokolov, J. Louko, S. Maniscalco, I. Vilja, Phys. Rev. D **101**, 024047 (2020)

IV **Pairwise tomography networks for many-body quantum systems**,
G. García-Pérez, M. A. C. Rossi, *B. Sokolov*, E.-M. Borrelli, S. Maniscalco, Phys. Rev. Research **2**, 023393 (2020)

V **Emergent entanglement structures and self-similarity in quantum spin chains**,
B. Sokolov, M. A. C. Rossi, G. García-Pérez, S. Maniscalco, arXiv:2007.06986 (2020).

Other published material

This is a list of the publications produced which have not been chosen as a part of this doctoral thesis

- **Revealing memory effects in phase-covariant quantum master equations**,
  J. Teittinen, H. Lyyra, *B. Sokolov*, S. Maniscalco, New J. Phys. **20**, 073012 (2018).

Introduction

This thesis has its roots in three different fields, general relativity, open quantum systems and complex network theory. The underlying goal is to use in a new way concepts and tools of one of these fields to better understand phenomena typical of the other field. The reason of this approach is twofold: on the one hand, there is hope to gain new insight and discover new phenomena by using tools previously unused in a given field; on the the other hand, the possibility of generalizing the toolbox itself based on new features arising from its applications in a new context is explored. As an example, the open quantum system approaches to study the Unruh effect as well as gravitationally induced time dilation are used. This allows one to see under a new light these effects for example describing for the first time information flow and memory effects in the context of non-inertial frames. Moreover, the complex network theory techniques to describe open quantum systems including the description of the environment have been used. This is pictorially illustrated in Figure 1. As will be described briefly later,

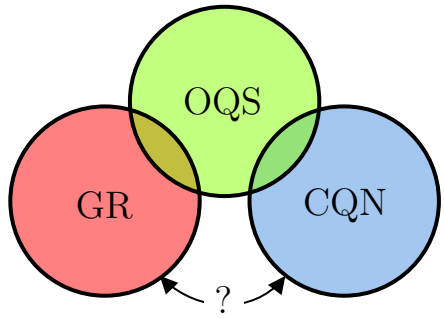

Figure 1: Sketch diagram of the interplay of main subjects of the thesis: general relativity, open quantum systems and complex quantum networks. The question mark between the lower two subjects indicates ground for future research.

the next future step is the connection between complex quantum networks and general relativity.

These efforts are part of the attempt to establish a new common framework with the long-term vision of tackling the long standing problem of giving a quantum mechanical description of general relativity. A possible path towards this vision is the connection between complex quantum networks and geometry through the concept of emergent geometry, which may in turn lead to a microscopic description of emergent spacetime [1]. The unification of quantum physics and general relativity is one of the most important challenges in physics and has been an open problem since the very birth of both theories. It may be therefore argued that a completely new perspective might be needed in order to discover new potential solutions. While this is beyond the scope of this thesis, some of the results and techniques that have been explored in the research articles adjacent to the thesis might contribute to such an ambitious scientific program.

The main results of this thesis are now briefly summarized and put into the context of the literature. Such results have been divided into two main groups. The first one has its core in open quantum systems theory applied to relativistic systems. The second one has its core in complex quantum networks used also for describing open quantum systems.

The first result (**Chapter 1**) in the first part of the thesis starts with a derivation of conditions for complete positivity - a feature of an operation on a quantum system which guarantees the physicality of such operation [2, 3]. This is important in light of various approximations taken in the derivation of equations of motion for quantum systems of specific types. The obtained results provide exact, analytical and easily verifiable conditions for physicality for a simple two-level quantum system subjected to a general phase covariant class of noise. These results are then used in the study of Unruh effect described in chapter 3.

The second result (**Chapter 2**) uses the open quantum systems tools in a different way compared to the conventional view. Indeed in this case the environment is not external, like an electromagnetic field, but instead is formed by the many internal degrees of freedom of the system itself. What is considered is a large molecule in a Schrödinger cat state, being a superposition of coherent wavepackets centered at different heights. In this case the open system is the center of mass while the environment is formed by the large number of vibrational degrees of freedom of the molecule. Our work generalizes the results of Ref. [4] by addressing two crucial points:

the use of a more physical description of the initial macroscopic superposition of distinguishable states and the holistic description of nonclassicality through a number of different indicators [5–9] which have been proposed in the literature over the years. In this sense time dilation induced decoherence is not seen just from one point of view but through different ideas of nonclassicality.

The last result (**Chapter 3**) of the first part of the thesis concerns the description of the dynamics of the Unruh effect in terms of information flow and backflow. Also in this case the starting point was the results of Ref. [10] which were then generalized to a more realistic scenario showing that a more accurate description leads to memory effects and non-Markovianity [11–15]. This is the first example in which the non-Markovianity measures, recently developed in open quantum systems to describe the memory effects in terms of information backflow, have been applied to the relativistic setting. Although the Unruh effect is not a consequence of general relativity, it is nevertheless closely related to the general relativistic Hawking radiation.

The second half of the thesis focuses on merging complex network theory [16] (**Chapter 4**) and quantum many-body physics. An efficient way of obtaining a network representation of many-body quantum states in terms of two-body reduced density operators (**Chapter 5**) has been discovered. Our algorithm reduces exponentially the number of measurement settings for pairwise quantities in many-body systems. By obtaining the reduced density operator for each pair of particles, one can calculate any pairwise quantity such as concurrence [17], mutual information [18], discord [19], classical correlations [20], etc. For each of these quantities one can construct a network where the nodes are each particle or spin and the weighted links are the values of the pairwise quantity. In our paper a multiplex of networks [21], where each layer indicates a pairwise network representation of a different quantity is also introduced. In the future, there are plans to study the correlations between different layers of a multiplex using tools of complex network theory to extract potentially useful additional information. The multiplex method has been used in our article, i.e., for characterizing the performance of small quantum computers, for describing the ground state of condensed matter spin systems and, interestingly, for investigating the interaction of a quantum system with its environment without neglecting the description of the environment itself. This latter example shows the connection between complex quantum network approaches and open

quantum systems. In other words, the claim is that the methods developed for complex quantum networks allow for a description of correlations between system and environment but also between different parts of the environment.

Finally, the last paper of the thesis (**Chapter 6**) explores a specific well-known and extensively studied spin model known as the XX model [22]. Previously unknown physical phenomena are discovered using complex network measures. Remarkably, emergent structure of entanglement can be detected with our approach. The concept of emergence is expected to play a key role in understanding how macroscopic properties and collective behavior appear from microscopic structures. This has potential impact in fields like quantum biology, quantum gravity, condensed matter physics and several others. The natural next step would be to use the complex network representation we have developed to simulate quantum field theory in curved space time (and specifically Hawking radiation of a black hole) according to the approach recently presented in Ref. [23]. This would allow us to perform the first step in establishing the missing link between complex quantum networks and general relativity.

Chapter 1

Open quantum systems

1.1 Quantum systems

Quantum mechanics is a fundamental paradigm of nature. It describes various phenomena and behaviors of particles on atomic and subatomic scales. The term *quantum* originates from the discretized, or quantized nature of atomic energy level differences and light particles (photons) [24]. In classical mechanics, a classical system is said to reside in a configuration called a *state*, which is a collection of parameters in some parameter space, capable of fully describing the possible behavior of that system given a set of physical laws that govern that behavior. The state can be a countable or, for example in case of fields, an uncountable set of values. A simple example of a state would be the set of position and momentum of a particle $(\bar{x}, \bar{p})$.

Similarly, a quantum system resides in a quantum state commonly denoted in a bra-ket notation as $|\psi\rangle$. It is a mathematical object that gives the probability distribution for the outcomes of measurements performed on the quantum system. Contrarily to the state of a classical system, the quantum state therefore does not need to have exactly defined values for its properties, providing that full information is known. Moreover, the quantum nature of the system dictates that some of its properties, such as position and momentum, cannot simultaneously have precisely defined values [25].

In mathematical terms, a *pure* quantum state $|\psi\rangle$ is a norm 1 vector in the Hilbert space of the system. A Hilbert space, denoted by $\mathcal{H}$, is an extention of Euclidean space which is complete and has a defined inner product. In the quantum case, the inner product is an L^2-product. As an example, the Hilbert space of a spin-$\frac{1}{2}$ particle such as an electron is $\mathbb{C}^2$, which means that all possible internal states of an electron exist in this

space only.

In the thesis, we shall refer to two-level systems, such as the electron spin, as qubits. Indicating with $|0\rangle$ and $|1\rangle$ an orthonormal basis of the Hilbert space of the qubit, its generic state of a qubit can be written as $|\psi\rangle = \alpha|0\rangle + \beta|1\rangle$, with $|\alpha|^2 + |\beta|^2 = 1$, and $\alpha, \beta \in \mathbb{C}$.

A system of n distinguishable particles forms a many-body system and its Hilbert space consists of tensor products of Hilbert spaces corresponding to each of the particles, namely, $\mathcal{H} = \mathcal{H}_1 \otimes \mathcal{H}_2 \otimes ... \otimes \mathcal{H}_n$. Considering many-body systems permits us to introduce a markedly quantum property called entanglement. This is a type of correlation between particles which is stronger than any classical correlation. For example, for a two-qubit system with Hilbert space $\mathcal{H}_A \otimes \mathcal{H}_B$, if the total state can be written as a product state $|\psi\rangle_A \otimes |\psi\rangle_B$, the state is called separable, as the dynamics can be explored independently. However, not all states are separable, a state such as

$$|\psi\rangle = \frac{1}{\sqrt{2}} \left(|0\rangle_A \otimes |1\rangle_B - |1\rangle_A \otimes |0\rangle_B\right) \tag{1.1}$$

cannot be written as a product state. States like these are called *entangled* states. For such an entangled state, it is not possible to attribute to either qubit A or B a definite pure state. The state of qubit A or qubit B is nevertheless a physical state which is a probabilistic mixture of pure states, known as *mixed* quantum state. The description of mixed states requires a generalization of mathematical description given so far. We therefore introduce the density matrix formalism in which the quantum state is usually written as a square density matrix ρ with the dimension $n \times n$ and $n^2 - 1$ independent components, where n is the dimension of the Hilbert space. The density matrix ρ is a trace 1 positive semi-definite operator of the form

$$\rho = \sum_{ij} p_{ij} |\psi_i\rangle\langle\psi_j|, \tag{1.2}$$

where, given that the vectors $|\psi_i\rangle$ are orthogonal to each other, p_{ii} are the probabilities of finding the system in the pure state $|\psi_i\rangle$ and $\langle\psi_j|$ is the conjugate of $|\psi_j\rangle$. The probabilities sum up to 1: $\sum_i p_{ii} = 1$. When the density ρ has rank 1, then the state is pure and can be described by the state vector formalism introduced above as $|\psi\rangle$. Extending the definition of separability given above for pure states, we say that a mixed state is

separable if

$$\rho = \sum_i p_i \rho_i^A \otimes \rho_i^B. \tag{1.3}$$

If a state cannot be cast in the form above, it is said to be entangled. In general, we indicate with $\rho_i^{A(B)}$ the state of system $A(B)$ obtained from the total state by the partial trace operation defined as

$$\rho_{A(B)} = Tr_{B(A)}[\rho] = \sum_j \langle j|_{B(A)} \rho |j\rangle_{B(A)}, \tag{1.4}$$

where $\left\{|j\rangle_{B(A)}\right\}_j$ is the orthonormal basis of system $B(A)$. In the case of the entangled state considered in Eq. (1.1), the reduced state ρ_A is of the form

$$\rho_A = \tfrac{1}{2}\left(|0\rangle_A\langle 0|_A + |1\rangle_A\langle 1|_A\right), \tag{1.5}$$

which is a mixed state as anticipated above [26].

To complete our short introduction to the key concepts of quantum theory, it is important to describe how quantum systems evolve in time. We begin by considering perhaps the most famous equation in quantum physics, the Schrödinger equation

$$i\hbar \frac{d}{dt}|\psi(t)\rangle = H|\psi(t)\rangle, \tag{1.6}$$

with H the Hamiltonian of the system [27]. In quantum mechanics, the Hamiltonian is constructed in a similar manner as in classical mechanics. However, while in classical mechanics, the Hamiltonian is a scalar-valued function, in quantum mechanics, it is an operator. The eigenvalues of H are the energy levels of the system. Equation (1.6) describes the time evolution of any initial pure state of a closed quantum system. A description of the Schrödinger equation in terms of the density matrix of a pure state, namely $\rho = |\psi\rangle\langle\psi|$, is the von Neumann equation written as

$$i\hbar \frac{d\rho(t)}{dt} = [H, \rho(t)]. \tag{1.7}$$

Due to its linear character, if any two states are solutions of the equa-

tion, then their superposition has to be a solution as well. The general solution of the Schrödinger equation is

$$|\psi(t)\rangle = U(t)|\psi(0)\rangle = e^{-\frac{i}{\hbar}Ht}|\psi(0)\rangle. \tag{1.8}$$

Due to Hermiticity of the Hamiltonian H, the time evolution operator $U(t)$ is unitary, meaning $U^\dagger = U^{-1}$. Therefore the dynamics of pure quantum states are reversible. If the quantum system is not closed, namely it interacts with its surroundings, then the state of the system is generally mixed and its dynamics are not described by the Schrödinger equation. We refer to such systems as open quantum systems and their dynamics follow the well known master equation. In the rest of this chapter we introduce the main properties of open quantum systems and describe the master equation formalism.

1.2 Why open quantum systems?

Real systems, classical or quantum, can said to be closed only up to a certain approximation which may or not be significant in describing the behaviors of these systems. All systems are embedded and, as a consequence, interacting with environments surrounding them. Generally, the total system comprising the open system and its environment is closed. It is therefore in principle possible to solve the dynamics of the whole system using the Schrödinger equation and then perform a partial trace over the environmental degrees of freedom. However, the environment generally possesses an extremely large number of degrees of freedom. Solving the dynamics of quantum systems of large amounts of constituents may be computationally intractable due to their sheer complexity. Moreover, for many quantum systems, the energies of individual particles comprising our system are usually on par with energies of particles of the environment, hence it is likely that the particles we are interested in would be perturbed by their environments. Finally, we should note that the experiments conducted on quantum systems are becoming more and more precise and noise-free, but it may be impossible to completely get rid of measurement apparatus related noise and is certainly impossible to get rid of everpresent vacuum fluctuations.

These considerations have contributed for the development in the research of the field of open quantum systems - quantum systems which are assumed to be interacting with their environment. During the last two

decades the theory of open quantum systems has received increasing attention due to its influence in the growing field of quantum technologies [11–15]. This is because noise induced by the environment has been considered for several years as the major enemy of sensitive quantum devices. Indeed as we see in chapters 1 and 2, decoherence induced by the environment rapidly destroys quantum properties which are a resource for quantum technologies. This has led to extensive experimental efforts aimed at modeling and mitigating environmental noise. It is nowadays recognized however that environmental noise can also be used to enhance or preserve quantum properties. The field of quantum reservoir engineering indeed focuses on suitably manipulating the environment in order to achieve particular quantum tasks.

In the following sections we will (i) introduce the microscopic derivation to the famous Gorini-Kossakowski-Sudarshan-Lindblad (GKSL) master equation [28, 29], (ii) define the dynamical map and its properties of complete positivity, divisibility and non-Markovianity, (iii) present our results on phase-covariant single qubit master equation.

1.3 GKSL master equation

In the microscopic approach to open quantum systems dynamics we start by modeling the total closed system, whose Hilbert space is $\mathcal{H}_S \otimes \mathcal{H}_E$, by means of the microscopic Hamiltonian

$$H = H_S \otimes I_E + I_S \otimes H_E + H_I, \tag{1.9}$$

where H_S and H_E are the free Hamiltonians of the system and of the environment, respectively, and H_I is the interaction term. The initial state of the total system is assumed to be separable, i.e., no correlations between system and environment are initially present. As the total system is closed, we can write its unitary evolution as

$$\rho_{SE}(t) = U(t)\,\rho_S(0) \otimes \rho_E\,U^\dagger(t), \tag{1.10}$$

with $U(t) = \exp[-iHt/\hbar]$. If we now take the partial trace over the environment in the equation above, we have:

$$\begin{aligned}\rho_S(t) &= \mathrm{Tr}_E\{U(t)\,\rho_S(0)\otimes\rho_E\,U^\dagger(t)\}\\ &\equiv \Lambda_t\rho_S(0),\end{aligned} \tag{1.11}$$

where Λ_t is the dynamical map. In the following we will describe the assumptions that allow us, starting from a microscopic description of system plus environment, to derive a physically meaningful master equation.

Let us consider the dynamics of the overall density operator ρ_{SE} given by the von Neumann equation which, in units of $\hbar$ and in the interaction picture, reads as follows:

$$\frac{d\rho_{SE}(t)}{dt} = -i[H_I(t),\rho_{SE}(t)], \tag{1.12}$$

where we omit for simplicity of notation the subscript I which we should use to indicate the density matrix in the interaction picture. The integral form of this equation is

$$\rho_{SE}(t) = \rho_{SE}(0) - i\int_0^t ds[H_I(s),\rho_{SE}(s)]. \tag{1.13}$$

Inserting Eq. (1.13) into Eq. (1.12) and taking the partial trace over the environmental degrees of freedom we get

$$\frac{d\rho_S}{dt}(t) = -\int_0^t ds\mathrm{Tr}_E\{[H_I(t),[H_I(s),\rho_{SE}(s)]]\}, \tag{1.14}$$

where we have assumed $\mathrm{Tr}_B[H_I(t),\rho_{SE}(0)] = 0$.

We assume now that system and environment are weakly coupled (Born approximation). This approximation amounts to assuming that the correlations established between system and environment are negligible at all times (initially zero), i.e.,

$$\rho_{SE}(t) \approx \rho_S(t)\otimes\rho_E$$

Within this approximation we get a closed integro-differential equation for

$\rho_S(t)$

$$\frac{d\rho_S(t)}{dt} = -\int_0^t ds \mathrm{Tr}_E\{[H_I(t), [H_I(s), \rho_S(s) \otimes \rho_E]]\} \tag{1.15}$$

Note that, in the equation above, the future evolution of the system, described by $\frac{d\rho_s}{dt}(t)$, depends on the past states of the system $\rho_S(s)$ for times $s < t$ through the integral. A further simplification to this equation is obtained by assuming that we can replace $\rho_S(s)$ appearing inside the integral with its value at time t, $\rho_S(t)$, which is possible if the density matrix does not change strongly in the interval of time $0 \leq s \leq t$. This is the case in many physical situations in which this integrand (or rather that part of it describing the environment correlations) quickly decays to zero after a short characteristic correlation time t_E. This timescale quantifies the memory time of the reservoir. Hence, if the density matrix of the system does not change sensibly in the correlation time t_E, then we can approximate $\rho_S(s)$ with $\rho_S(t)$ in Eq. (1.15). The resulting equation is known as the Redfield equation

$$\frac{d\rho_S(t)}{dt} = -\int_0^t ds \mathrm{Tr}_E\{[H_I(t), [H_I(s), \rho_S(t) \otimes \rho_E]]\}. \tag{1.16}$$

Equation (1.16) is local in time, i.e., the future evolution of the state of the system does not depend on its past state. However, it still retains memory of the initial state $\rho_S(0)$.
Until now we have assumed the density matrix does not change much within the correlation time t_E. The next step will be to neglect such a change altogether by performing a coarse graining in time. This is mathematically achieved by doing a change of variable $s \to t - s$ and replacing the upper limit of the integral in Eq. (1.16) with ∞,

$$\frac{d\rho_S(t)}{dt} = -\int_0^\infty ds \mathrm{Tr}_E\{[H_I(t), [H_I(t-s), \rho_S(t) \otimes \rho_E]]\}, \tag{1.17}$$

The two-step approximation described in Eqs. (1.16) and (1.17) is known as the Markov approximation. We say that Eq. (1.17) is derived from a microscopic model under the Born-Markov approximation, i.e., for weak coupling and quickly decaying reservoir correlations (memoryless dynamics).

Let us decompose the interaction Hamiltonian H_I in terms of operators

of the system and of the environment:

$$H_I = \sum_\alpha A_\alpha \otimes B_\alpha,$$

with A_α (B_α) Hermitian operators of the system (environment).

Let us assume that H_S has a discrete spectrum and let us indicate with ϵ the eigenvalues and with $\Pi(\epsilon)$ the corresponding projectors into the corresponding eigenspace. We define the eigenoperators of the system as follows

$$A_\alpha(\omega) = \sum_{\epsilon' - \epsilon = \omega} \Pi(\epsilon) A_\alpha \Pi(\epsilon'). \tag{1.18}$$

We can rewrite the interaction Hamiltonian in terms of eigenoperators of H_S, and then pass to the interaction picture exploiting the fact that the system eigenoperators have a simple time dependency in this picture. The environment operators in the interaction picture are simply given by $B_\alpha(t) = e^{iH_E t} B_\alpha e^{-iH_E t}$.

After some algebra, we can rewrite the master equation in the following form

$$\frac{d\rho_s(t)}{dt} = \sum_{\omega,\omega'} \sum_{\alpha,\beta} e^{i(\omega'-\omega)t} \Gamma_{\alpha\beta}(\omega) [A_\beta(\omega)\rho_S(t) A_\alpha^\dagger(\omega') - A_\alpha^\dagger(\omega') A_\beta(\omega)\rho_S(t)] + \text{h.c.} \tag{1.19}$$

where we introduced

$$\Gamma_{\alpha\beta}(\omega) \equiv \int_0^\infty ds e^{i\omega s} \langle B_\alpha^\dagger(t) B_\beta(t-s)\rangle,$$

with the reservoir correlation functions given by

$$\langle B_\alpha^\dagger(t) B_\beta(t-s)\rangle \equiv \mathrm{Tr}_E\{B_\alpha^\dagger(t) B_\beta(t-s)\rho_E\}.$$

Such correlation functions are homogeneous in time if the reservoir is stationary, i.e.,

$$\langle B_\alpha^\dagger(t) B_\beta(t-s)\rangle = \langle B_\alpha^\dagger(s) B_\beta(0)\rangle. \tag{1.20}$$

We now make the last approximation, known as the secular approxima-

tion. First we define t_S as the characteristic intrinsic evolution time of the system. This timescale is generally of the order of $t_S \approx |\omega' - \omega|^{-1}, \omega' \neq \omega$. We indicate with t_R the relaxation time of the open system. If $t_S \gg t_R$ we can neglect all the exponential terms oscillating at frequency $|\omega' - \omega| \neq 0$ as they oscillate very rapidly (averaging out to zero) over the timescale t_R over which ρ_S changes appreciably. We then decompose the environment correlation functions into their real and imaginary parts

$$\Gamma_{\alpha\beta}(\omega) = \frac{1}{2}\gamma_{\alpha\beta}(\omega) + iS_{\alpha\beta}(\omega),$$

where, for fixed ω,

$$\gamma_{\alpha\beta}(\omega) = \Gamma_{\alpha\beta}(\omega) + \Gamma^*_{\beta\alpha}(\omega) = \int_{-\infty}^{+\infty} ds e^{i\omega s} \langle B^\dagger_\alpha(t-s) B_\beta(t) \rangle,$$

form a positive-semidefinite matrix and

$$S_{\alpha\beta}(\omega) = \frac{1}{2i}[\Gamma_{\alpha\beta}(\omega) - \Gamma^*_{\beta\alpha}(\omega)],$$

form a Hermitian matrix. With these definitions we finally arrive at the interaction picture master equation

$$\frac{d\rho_S(t)}{dt} = -i[H_{LS}, \rho_S(t)] + \mathcal{L}(\rho_S(t)), \tag{1.21}$$

where

$$H_{LS} = \sum_\omega \sum_{\alpha,\beta} S_{\alpha\beta}(\omega) A^\dagger_\alpha(\omega) A_\beta(\omega),$$

is a Lamb shift term which provides a Hamiltonian contribution to the dynamics and

$$\mathcal{L}(\rho_S) = \sum_\omega \sum_{\alpha,\beta} \gamma_{\alpha\beta}(\omega) \left[A_\beta(\omega) \rho_S A^\dagger_\alpha(\omega) - \frac{1}{2}\{A^\dagger_\alpha(\omega) A_\beta(\omega), \rho_S\} \right].$$

This form of the dissipator (generator of the dynamics) $\mathcal{L}$ is known as first standard form. Diagonalizing the real positive-semidefinite matrix $\gamma_{\alpha\beta}(\omega)$

we get the GKSL Markovian master equation

$$\mathcal{L}(\rho_S) = \sum_{\omega} \sum_{\alpha} \gamma_\alpha(\omega) \left[\bar{A}_\alpha(\omega) \rho_S \bar{A}_\alpha^\dagger(\omega) - \frac{1}{2} \{ \bar{A}_\alpha^\dagger(\omega) \bar{A}_\alpha(\omega), \rho_S \} \right].$$

In general, the procedure described above allows us to derive microscopically the GKSL Markovian master equation for any open quantum system. The assumptions of the derivation are: uncorrelated system-environment initial conditions, weak coupling between system and environment, rapidly decaying system and environment correlations and the secular approximation. Under these conditions, open quantum systems are described by the following master equation

$$\frac{d\rho(t)}{dt} = -i[H, \rho] + \sum_k \gamma_k \left(V_k \rho V_k^\dagger - \frac{1}{2} \{ V_k^\dagger V_k, \rho \} \right) \equiv L(\rho), \tag{1.22}$$

where H includes the Lamb shift Hamiltonian, $\gamma_k \geq 0$ are the decay rates and V_k are the so called Lindblad or jump operators. The jump operators span the space of operators O in the Hilbert space of the generator $\mathcal{L}$ under the condition $\mathrm{Tr}[O^\dagger O] < \infty$ forming the *Liouville space*. $L(\rho)$ is also known as the generator of the open quantum system dynamics. We note here that the master equation (1.22) comprises of two terms, the first one describes the unitary dynamics and the second one describes the non-unitary dynamics arising due to interaction with the environment. A more general form of master equation can be obtained releasing some of the approximations considered in the microscopic derivation. In this thesis, we will describe such more general systems and we therefore introduce here the corresponding master equation:

$$\frac{d\rho(t)}{dt} = -i[H, \rho] + \sum_k \gamma_k(t) \left(V_k \rho V_k^\dagger - \frac{1}{2} \{ V_k^\dagger V_k, \rho \} \right) \equiv L_t(\rho). \tag{1.23}$$

Equations of this form are known as a particular case of the time-local master equations [30]. In equation (1.23) whenever $\gamma_k(t) \geq 0$, the dynamics is said to be divisible. In the opposite case, if $\gamma_k(t)$ takes negative values, the dynamics is said to be non-divisible. We will further describe these differences in the next section.

1.4 Dynamical maps

By a general quantum evolution we mean a dynamical map Λ_t which maps an initial state ρ into an evolved state $\rho_t := \Lambda_t(\rho)$ and hence provides the natural generalization of the unitary evolution $\rho_t = \mathcal{U}_t(\rho)$.

Mathematically, the dynamical map, is a family of maps $\Lambda_t : M_n(\mathbb{C}) \to M_n(\mathbb{C})$ parametrized by time $t \geq 0$ such that $\Lambda_0 = I_n$.

Consider a linear map $\Lambda_t : M_n(\mathbb{C}) \to M_n(\mathbb{C})$ and let $M_n^+(\mathbb{C}) = \{A \in M_n(\mathbb{C}) \,|\, A \geq 0\} \subset M_n(\mathbb{C})$ be a convex subset of positive-semidefinite matrices. The dynamical map Λ_t transforms physical states into other physical states and it must satisfy the following properties

- positive: $\Lambda_t(M_n^+(\mathbb{C})) \subset M_n^+(\mathbb{C})$,
- trace-preserving: $\operatorname{Tr} \Lambda_t(A) = \operatorname{Tr} A$.

The possible presence of entanglement between the open system and larger parts of the environment imposes a stricter condition than positivity, namely complete positivity. Broadly speaking, complete positivity ensures the physicality of any system which contains our quantum system. This is defined as follows: Λ_t is completely positive iff for all $k \in \mathbb{N}$

$$I_k \otimes \Lambda_t : M_k(\mathbb{C}) \otimes M_n(\mathbb{C}) \to M_k(\mathbb{C}) \otimes M_n(\mathbb{C}) \tag{1.24}$$

is positive. The dynamical map defines the family of solutions of the master equation for an open quantum system, such as for example Eq. (1.23). Specifically, in the time-local case,

$$\Lambda_t = \mathrm{T} \exp\left(\int_0^t L_\tau \, d\tau \right), \tag{1.25}$$

where T denotes the chronological ordering operator. The above formula is defined by the following Dyson series

$$\Lambda_t = I_n + \int_0^t dt_1 \, L_{t_1} + \int_0^t dt_1 \int_0^{t_1} dt_2 \, L_{t_1} \, L_{t_2} + \dots \, , \tag{1.26}$$

provided that it converges.

1.5 Non-Markovianity

The concept of Markovian and non-Markovian stochastic process has a clear and rigorous formulation in the classical domain. The extension to quantum processes and dynamics, however, is not straightforward. Open quantum systems, indeed, may display dynamical features which do not have a classical counterpart, such as re-coherence, information trapping, entanglement sudden death and revivals, and so on [15]. For this reason, the generalization of the definition of Markovian/non-Markovian process from classical to quantum is still the subject of an intense debate [12, 14]. Generally speaking, two approaches to the definition of quantum non-Markovianity are dominant. The first one focuses on the properties of the master equation or the corresponding dynamical map, while the second one emphasizes the need of a more physical approach, identifying memory effects and non-Markovianity with the occurrence of information back-flow. The latter approach does not require the knowledge of the explicit form of either the master equation or dynamical map, and has been pioneered by Breuer, Laine and Piilo, who introduced the now famous BLP non-Markovianity measure [11].

Historically, Markovian open quantum dynamics was identified with the GKSL form of the master equation and was extensively used due to its powerful property of guaranteeing complete positivity (CP), and hence physicality, of all the solutions at all times. A straightforward extension of the GKSL theorem to time-local master equations identifies Markovian and non-Markovian dynamics with the properties of the dynamical map Λ_t : $\rho(t) = \Lambda_t \rho(0)$ characterizing the open system evolution. More precisely, the dynamics is said to be Markovian whenever the dynamical map possesses the property of being completely-positive (CP) divisible, namely whenever the propagator $V_{t,s}$, defined by $\Lambda_t = V_{t,s}\Lambda_s$, is CP. On the contrary, non-Markovian dynamics occurs when the dynamical map Λ_t is not CP divisible. For time-local master equations defined in Eq. (1.23), it is possible to show that the corresponding dynamical map satisfies divisibility if and only if $\gamma_k(t) \geq 0$. If on the other hand, $\gamma_k(t)$ becomes temporarily negative, there will exist an intermediate map $V_{t,s}$ which is not completely positive and trace preserving (CPTP), defying the composition law. Hence, the dynamics is not divisible.

The evolution of a quantum system interacting with its surrounding environment, be it classical or quantum, relativistic or non-relativistic, can

be described in terms of exchange of energy and/or information between the two interacting parties. While the concept of energy is uniquely defined in quantum systems, a unique definition of information is lacking. Indeed, in principle, there are a number of useful and rigorous choices for quantifying information, and hence information flow, and such choices obviously depend on which "type" of information one is interested in. Quantum information theory deals with the study of information quantifiers, their properties, their dynamics, and their usefulness in quantum computation, communication, metrology and sensing. In the following we will recall the main non-Markovianity measures based on information flow.

The first attempt to quantify system-environment information flow, and connect it to the Markovian or non-Markovian nature of the dynamics, was based on the concept of trace distance between two states ρ_1 and ρ_2 of an open system,

$$D(\rho_1, \rho_2) = \tfrac{1}{2}\mathrm{tr}|\rho_1 - \rho_2|. \tag{1.27}$$

The trace distance is invariant under unitary transformations and contractive for CP dynamical maps, i.e., given two initial open-system states $\rho_1(0)$ and $\rho_2(0)$, the trace distance between the time-evolved states never exceeds its initial value $D[\rho_1(t), \rho_2(t)] \leq D[\rho_1(0), \rho_2(0)]$.

Trace distance is a measure of information content of the open quantum system since it is simply related to the maximum probability P_D to distinguish two equiprobable quantum states in a single-shot experiment, namely $P_D = \frac{1}{2}[1 + D(\rho_1, \rho_2)]$ [31]. Therefore, an increase in trace distance signals an increase in our information about which one of the two possible states the system is in. One can define information flow as the derivative of trace distance as follows:

$$\sigma(t) = \frac{d}{dt} D[\rho_1(t), \rho_2(t)]. \tag{1.28}$$

Even though trace distance cannot increase under CP maps, it may not behave always in a monotonic way as a function of time. Specifically, whenever the trace distance decreases monotonically, information flow is negative, meaning that the system continuously loses information due to the presence of the environment. On the other hand, if for certain time

intervals information flow becomes positive, then this signals a partial and temporary increase of distinguishability and, correspondingly, a partial recover of information. This information back-flow has been proposed as the physical manifestation of memory effects and non-Markovianity. This idea is known as BLP non-Markovianity.

Note that, whenever the dynamical map is BLP non-Markovian, i.e., in presence of information back-flow, then it is also CP non-divisible. However, the inverse is not true, namely, there exist systems that are CP non-divisible but BLP Markovian. In general, the concept of non-divisibility and the concept of BLP non-Markovianity, or information back-flow quantified by trace distance, do not coincide and their relationship has been the subject of numerous studies [13].

Based on this approach, the BLP measure of non-Markovianity $\mathcal{N}_{\mathrm{BLP}}$ is defined by summing over all periods of non-monotonicity of the information flow, including an optimization over all pairs of initial states of the system:

$$\mathcal{N}_{\mathrm{BLP}}(\Phi_t) = \max_{\rho_{1,2}(0)} \int_{\sigma>0} dt\, \sigma(t). \tag{1.29}$$

The difference between the concept of CP divisibility and the concept of memory effects due to information backflow, as signaled by an increase of distinguishability, can be overcome if one allows for a more general definition of distinguishability between states. More precisely, the concept of distinguishability based on trace distance is based on the idea of equal probabilities of preparing the two states, i.e., the preparation is uniformly random and there is no prior additional information on which one of the two states is prepared. One can, however, generalize this concept by introducing the Helstrom matrix Δ,

$$\Delta = p_1\rho_1 - p_2\rho_2, \tag{1.30}$$

where p_1 and p_2 are the prior probabilities of the corresponding states. The information interpretation in terms of the one-shot two-state discrimination problem is valid also in this more general setting [32].

In more detail, one now considers two states and their corresponding ancilla evolving under the completely positive, trace preserving dynamical

map Λ_τ as follows

$$\tilde{\rho}_{1,2}(t) = (\Lambda_\tau \otimes \mathcal{I}_d)\tilde{\rho}_{1,2}(0), \tag{1.31}$$

with $\tilde{\rho}_{1,2}$ the combined system-ancilla state, $\mathcal{I}_d$ the identity map, and d the dimension of the Hilbert space of the system, which in this case is equal to the one of the ancilla.

It has been recently shown in Ref. [32] that, for bijective maps, the trace norm of the Helstrom matrix defined as,

$$E(t) = |\Delta(t)| = |p_1\tilde{\rho}_1(t) - p_2\tilde{\rho}_1(t)|, \tag{1.32}$$

is monotonically decreasing $\forall p_i, \tilde{\rho}_i(t)$ iff the map is CP divisible. This result has been generalized to nonbijective maps in Ref. [33]. This allows one to interpret lack of CP divisibility in terms of information backflow for system and ancilla, when having prior information on the state of the system in the form of unequal probabilities $p_{1,2}$.

Finally, one can release the assumption of prior information and prove that, if one uses a $d+1$ dimensional ancilla, then the dynamical map Λ_τ is CP divisible if and only if the trace distance D decreases or remains constant as a function of time for all pairs of initial system-ancilla states Ref. [34]. Therefore, also in this case, one can interpret the loss of CP divisibility in terms of information backflow for the system-ancilla pair. For further details on the connection between CP divisibility and information backflow we refer the reader to the recent perspective article [15].

1.6 Phase-covariant time-local qubit dynamics

In this section we summarize the result of paper (I) and introduce the time-local phase-covariant master equation for a qubit. Our main result is the analytical solution of the model and the derivation of complete positivity conditions. In the paper we also discuss the effects of temperature on the non-Markovian behaviour of the system as well as noise additivity properties.

Let us consider the following time-local master equation for the qubit

density matrix ρ in the interaction picture and in units of $\hbar$,

$$\begin{aligned}\frac{d\rho}{dt} &= L_t(\rho) \equiv -i\omega(t)\left[\sigma_z,\rho\right] + \frac{\gamma_1(t)}{2}L_1(\rho) + \frac{\gamma_2(t)}{2}L_2(\rho) \\ &+ \frac{\gamma_3(t)}{2}L_3(\rho), \end{aligned} \tag{1.33}$$

where $\gamma_i(t)$ are time-dependent rates, $\omega(t)$ is a time-dependent frequency shift, and the dissipators $L_i(\rho)$ are defined as

$$\begin{aligned} L_1(\rho) &= \sigma_+\rho\sigma_- - \tfrac{1}{2}\left\{\sigma_-\sigma_+,\rho\right\}, \\ L_2(\rho) &= \sigma_-\rho\sigma_+ - \tfrac{1}{2}\left\{\sigma_+\sigma_-,\rho\right\}, \\ L_3(\rho) &= \sigma_z\rho\sigma_z - \rho. \end{aligned} \tag{1.34}$$

In the equations above $\sigma_\pm = \sigma_x \pm i\sigma_y$ are the inversion operators and σ_i $(i = x, y, z)$ are the Pauli operators. The three dissipators L_1, L_2, L_3, describe heating, dissipation and dephasing, respectively. The master equation (1.33) describes phase covariant noise and has been considered recently in the context of quantum metrology in noisy channels [35, 36]. Here, phase-covariant refers to dynamical maps Λ_t that commute with rotations $R_z(\theta)$ with respect to z-axis of the Bloch sphere:

$$\Lambda_t R_z(\theta) = R_z(\theta)\Lambda_t \forall\theta. \tag{1.35}$$

The solution of master equation in Eq. (1.33) has been derived in paper (I) and is given for the ground state probability $\rho_{00} = \langle 0|\rho(t)|0\rangle$ and the coherence $\rho_{01} = \langle 0|\rho(t)|1\rangle$ by

$$\frac{d\rho_{00}}{dt} + \frac{\gamma_1(t)+\gamma_2(t)}{2}\rho_{00}(t) = \frac{\gamma_2(t)}{2}, \tag{1.36}$$

$$\frac{d\rho_{01}}{dt} = \rho_{01}(t)\left[2i\omega(t) + \frac{1}{2}\left(\frac{\gamma_1(t)+\gamma_2(t)}{2} + 2\gamma_3(t)\right)\right]. \tag{1.37}$$

The equations above are linear first-order differential equations and can be solved for any values of the time-dependent decay rates. The solution reads as follows:

$$\rho_{00}(t) = e^{-\Gamma(t)}\left[G(t) + \rho_{00}(0)\right], \tag{1.38}$$

$$\rho_{01}(t) = \rho_{01}(0)e^{i\Omega(t)-\Gamma(t)/2-\tilde{\Gamma}(t)}, \tag{1.39}$$

where

$$\Gamma(t) = \int_0^t dt'[\gamma_1(t') + \gamma_2(t')]/2, \tag{1.40}$$

$$\tilde{\Gamma}(t) = \int_0^t dt'\gamma_3(t'), \tag{1.41}$$

$$\Omega(t) = \int_0^t dt'\omega(t'), \tag{1.42}$$

$$G(t) = \int_0^t dt' e^{\Gamma(t')}\gamma_2(t')/2. \tag{1.43}$$

If the time-dependent coefficients quickly attain a stationary positive constant value, after an initial short time interval τ_c, known as the correlation time of the environment, one obtains the approximated GKSL master equation by coarse-graining over τ_c and finding the asymptotics for $t \gg \tau_c$ in Eqs. (1.40) - (1.42). More precisely one obtains the following Markovian, asymptotic limits for the quantities defined in Eqs. (1.40) - (1.43).

$$\Gamma_M = (\gamma_1 + \gamma_2)t/2, \tag{1.44}$$

$$\tilde{\Gamma}_M = \gamma_3 t, \tag{1.45}$$

$$\Omega_M = \omega t, \tag{1.46}$$

$$G_M = \frac{\gamma_2}{\gamma_1 + \gamma_2}\left(e^{(\gamma_1+\gamma_2)t/2} - 1\right). \tag{1.47}$$

Using these expressions one can recover the well known Markovian formulas for populations and coherences

$$\rho_{00}(t) = e^{-(\gamma_1+\gamma_2)t/2}\rho_{00}(0) + \frac{\gamma_2}{\gamma_1 + \gamma_2}\left(1 - e^{-(\gamma_1+\gamma_2)t/2}\right), \tag{1.48}$$

$$\rho_{01}(t) = \rho_{01}(0)e^{i\omega t - (\gamma_1+\gamma_2)t/4 - \gamma_3 t}. \tag{1.49}$$

We now introduce a heuristic model for the decay rates, allowing us to go beyond the weak coupling approximation. We assume that the open quantum system of interest is coupled to a thermal reservoir at the same temperature T. For the sake of clarity we disregard the dephasing term in the following description, for effects of the dephasing term we refer the reader to paper (I). The thermal reservoir induces heating and dissipation at rates given by $\gamma_1(t)/2 = Nf(t)$ and $\gamma_2(t)/2 = (N+1)f(t)$, with N the mean number of excitations in the modes of the thermal environment. We

notice that, for a zero T environment, the heating rate $\gamma_1(t) = 0$ while the dissipation rate $\gamma_2(t) = f(t)$. Hence, we consider as a possible physically reasonable choice for the time-dependent function $f(t)$ the one obtained in the exactly solvable zero-T model presented, e.g., in Ref. [37]. In this model the function $f(t)$ takes the form

$$f(t) = -2\mathrm{Re}\left\{\frac{\dot{c}(t)}{c(t)}\right\}, \tag{1.50}$$

with

$$c(t) = e^{-t/2}\left[\cosh(dt/2) + \frac{\sinh(dt/2)}{d}\right]c(0), \tag{1.51}$$

where $d = \sqrt{1-2R}$, and R is a dimensionless positive number measuring the overall coupling between the two-state system and the environment with respect to the width of the spectral density of the environment.

It is straightforward to see by explicitly calculating the decay rates $\gamma_1(t)$ and $\gamma_2(t)$ that they are always positive whenever $R < 1/2$ (divisible dynamics) and attain temporarily negative values for $R > 1/2$ (non divisible dynamics). Hence this model allows us to explore the transition between Markovian and non-Markovian dynamics by tuning the parameter R.

One obtains the following analytic expression for the ground state population

$$\rho_{00}(t) = x(t)^{2N+1}\rho_{00}(0) + \frac{N+1}{2N+1}\left(1 - x(t)^{2N+1}\right), \tag{1.52}$$

where we have used Eq. (1.50) and defined $x(t) = [c(t)/c(0)]^2$.

In Fig. 1.1 we plot the time evolution of the ground state population $\rho_{00}(t)$ (labeled as $P_1(t)$ as a function of time for different temperatures, i.e., N, in both the Markovian case, Fig. 1.1 (a), and the non-Markovian case, Fig. 1.1 (b). We notice that, for $R \gg 1$ and for increasing values of temperature, the oscillations in ground state population are quickly damped, even if the dynamics continues to be non-Markovian because both the $\gamma_1(t)$ and the $\gamma_2(t)$ decay rates take negative values. Hence, the presence of oscillations in the ground or excited state probability is not just connected to the Markovian or non-Markovian character of the dynamics, as it was for the exact model valid for $T = 0$ described in Ref. [37], but depends also on the temperature of the environment.

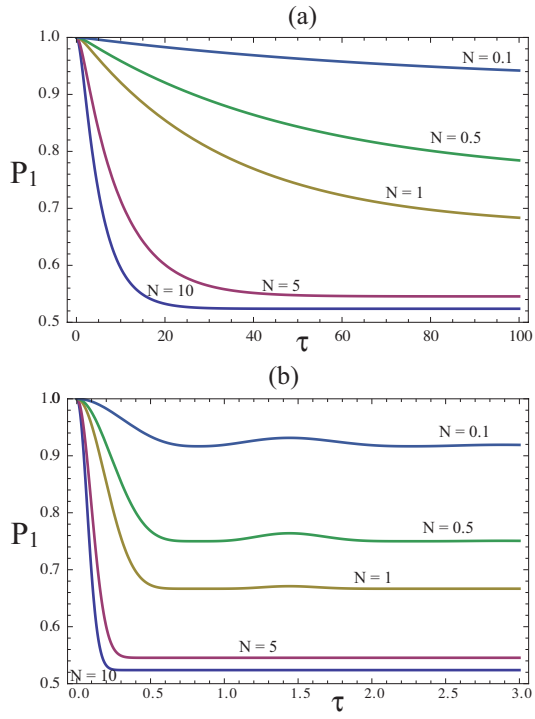

Figure 1.1: Dynamics of the ground state population $\rho_{00}(t)$ (labeled as $P_1(t)$) (a) in the weak coupling (Markovian) regime, $R = 0.01$, and (b) in the strong coupling (non-Markovian) regime, $R = 10$, for different values of N (temperature).

It is worth mentioning that conditions for complete positivity need to be examined in order to guarantee the physicality of the dynamics. This is because the decay rates temporarily take negative values and therefore do not satisfy the GKSL theorem. In paper (I) we have derived conditions for complete positivity in the form of inequalities involving the time dependent decay rates appearing in the master equation. Remarkably, for the example considered above, the system always satisfies the complete positivity conditions.

Chapter 2

Decoherence in a gravity field

2.1 Gravitational time dilation

To begin the discussion of gravitationally induced effects on quantum systems, it is clarifying to start from the special theory of relativity [38]. A product of centuries of scientific work, finally formulated by A. Einstein in Refs. [39, 40], special theory of relativity describes relations of laws of nature under Lorentz transformations, which are a group of space-time coordinate transformations, transforming a system of space-time coordinates x^α into another system x'^α as follows

$$x'^\alpha = \Lambda^\alpha_\beta x^\beta + a^\alpha, \tag{2.1}$$

where a^α and Λ^α_β are constants. These constants satisfy the conditions

$$\Lambda^\alpha_\gamma \Lambda^\beta_\delta \eta_{\alpha\beta} = \eta_{\gamma\delta}, \tag{2.2}$$

where,

$$\eta = \begin{pmatrix} 1 & 0 & 0 & 0 \\ 0 & -1 & 0 & 0 \\ 0 & 0 & -1 & 0 \\ 0 & 0 & 0 & -1 \end{pmatrix}, \tag{2.3}$$

is called the Minkowski metric tensor, or shortly, the Minkowski metric[1]. Note that in this section we use units $c = 1$ for brevity and in the whole chapter the Minkowski spacetime signature $(+,-,-,-)$. The indexed notation is common in works on theory of relativity and is a concise way of writing high-dimensional objects and tensor contractions. Whenever an index appears twice in the same equation, it is assumed to be summed over. Generally, Latin letters in indices label a 3-dimensional space, while Greek letters indicate a 4-dimensional spacetime, however this is always context- and metric-dependent.

One fundamental property of the Lorentz transformation is the invariance of *proper time* $d\tau$:

$$d\tau^2 \equiv dt^2 - d\mathbf{x}^2 = -\eta_{\alpha\beta} dx^\alpha dx^\beta = dt'^2 - d\mathbf{x}'^2 = d\tau'^2. \tag{2.4}$$

This property indicates that the speed of light is the same in all inertial systems. It can also be used to show the time dilation effect of moving clocks in special relativity:

Assume there are two clocks both beating at frequency ω and an observer who is at rest with respect to one of the clocks, and moving at speed $\mathbf{v}$ with respect to the other. The observer will see the first clock beating with a space-time interval $d\mathbf{x} = 0, dt = 1/\omega$, so the proper time interval will be $d\tau = \sqrt{dt^2 - d\mathbf{x}^2} = 1/\omega$. For a moving clock, $\mathbf{v}' = d\mathbf{x}'/dt'$, the proper time interval will be

$$d\tau' = \sqrt{dt'^2 - d\mathbf{x}^2} = \sqrt{dt'^2 - \mathbf{v}^2 dt'^2} = \sqrt{1 - \mathbf{v}^2}\, dt'. \tag{2.5}$$

As the coordinates of both clocks are a Lorentz transformation away from each other, we can set $d\tau' = d\tau$ and derive the observed frequency ω' of the second clock from the period $dt' = 1/\omega'$:

$$d\tau = \frac{1}{\omega} = \sqrt{1 - \mathbf{v}^2}\frac{1}{\omega'} \tag{2.6}$$

$$\Rightarrow \omega' = \omega\sqrt{1 - \mathbf{v}^2}. \tag{2.7}$$

This shows that the time measured by an observer using similar clocks depends directly on their observer-relative velocities. Equivalently, the above logic applies to a situation with two observers moving at different velocities

[1] A metric is a function which defines distances and angles on a surface.

and observing a single clock.

The metric in Eq. (2.3) is valid for a completely flat spacetime. It is therefore necessary to generalize the metric to a curved spacetime, such as one in a presence of a massive object. We can, however, use the equivalence principle to construct a locally inertial coordinate system and define proper time with the help of a general metric $g_{\mu\nu}$:

$$d\tau^2 = -g_{\mu\nu}dx^\mu dx^\nu. \tag{2.8}$$

Assuming that the clock is at rest, we can use Eq. (2.8) to obtain the metric-dependent form for the clock frequency:

$$\frac{d\tau^2}{dt^2} = -g_{00}\underbrace{\frac{dt}{dt}\frac{dt}{dt}}_{=1} - g_{ij}\underbrace{\frac{dx^i}{dt}\frac{dx^j}{dt}}_{=0 \text{ at rest}} \tag{2.9}$$

$$\begin{aligned} \Rightarrow d\tau^2 &= -g_{00}dt^2 \\ &= -g_{00}\frac{1}{\omega^2} \end{aligned} \tag{2.10}$$

To proceed further, we need to specify some details, such as the way we are measuring the clock frequency ω and the type of metric. A suitable metric defined in spherical coordinates is the Schwarzschild metric, defined with the line element of the proper time as

$$\begin{gathered} d\tau^2 = \underbrace{-\left(1-\frac{r_s}{r}\right)}_{=g_{00}(r)}dt^2 + \left(1-\frac{r_s}{r}\right)^{-1}dr^2 + r^2(d\theta^2+\sin^2(\theta)d\phi^2), \\ r_s = 2GM. \end{gathered} \tag{2.11}$$

The Schwarzschild metric assumes a spherically symmetric object of mass M and is valid for radii $r > r_s$, r_s being the Schwarzschild radius and G being the gravitational constant. We can now use the proper time equivalence

to directly compare frequencies ω_1, ω_2 at two radii r_1, r_2:

$$\begin{aligned} -\frac{g_{00}(r_1)}{\omega_1^2} &= -\frac{g_{00}(r_2)}{\omega_2^2} \\ \Rightarrow \frac{\omega_1}{\omega_2} &= \frac{g_{00}(r_2)}{g_{00}(r_1)} = \frac{1 - r_s/r_2}{1 - r_s/r_1} \\ &\approx 1 + r_s \left(r_1^{-1} - r_2^{-1} \right), \end{aligned} \tag{2.12}$$

where in the last approximation we have assumed $r_s \ll r_i$, i.e. both radii are much larger than the Schwarzschild radius. This shows that the relative running rates of these two clocks depend on their distance from the center of mass at $r = 0$.

Although the change in frequency is extremely small for reasonable clock separations and a gravitational field comparable to that produced by the planet Earth, this effect has been experimentally measured to the precision of height difference of 2 cm using atomic clocks [41, 42]. This makes the effect potentially meaningful for sensitive quantum systems as it can have an influence on quantum interference.

2.2 Open quantum system in presence of gravity

The environment of an open quantum system, although modeled as particles, does not have to be composed of external particles, but can emerge through interactions between various degrees of freedom of the system. This was the case explored in Refs. [4, 43], where the authors chose as the open system the position in the gravitational gradient of the center of mass of a many-body system. The internal degrees of freedom of this system, represented as harmonic oscillators of various frequencies, act as the environment. Gravitationally induced decoherence occurs when the initial state of the centre of mass is a superposition of eigenstates of the position operator $|\psi_{\text{cm}}(0)\rangle = \frac{1}{\sqrt{2}}(|x_1\rangle + |x_2\rangle)$.

In our work we took a modified approach, taking a superposition of two macroscopically distinguishable coherent states of the c.m. motion a.k.a. the Schrödinger cat state as the initial state. The center of mass motion is now described using creation $a^\dagger$ and annihilation a operators (a.k.a. ladder operators) by $H_{\text{cm}} = \hbar\omega_0 a^\dagger a$, ω_0 being the oscillator frequency.

The total Hamiltonian is then

$$H = H_{\rm cm} + H_0 + H_{\rm I}, \tag{2.13}$$

where, for $\Delta x_0 \equiv \sqrt{\frac{\hbar}{m\omega_0}}$ being the width of the ground state wavefunction,

$$H_0 = \sum_{i=1}^{N} \hbar\omega_i n_i, \tag{2.14}$$

$$H_{\rm I} = \Phi(X)\frac{H_0}{c^2} \equiv \hbar\Delta x_0 \frac{gX}{c^2}\left(\sum_{i=1}^{N}\omega_i n_i\right). \tag{2.15}$$

The constant g is the gravitational acceleration, H_0 is the Hamiltonian of the internal degrees of freedom described by N quantum harmonic oscillators of frequencies ω_i and $H_{\rm I}$ is the coupling between position x and internal energy H_0 to the lowest order in c^{-2}, induced by gravitational time-dilation and defined using the dimensionless position operator

$$X = \frac{1}{\sqrt{2}}(a^\dagger + a). \tag{2.16}$$

Assuming no initial correlations between system and environment, initially thermalized state of the internal degrees of freedom, a weak coupling limit, a massive system with mass m and $\rho(t) \approx \rho_{\rm cm}(t) \otimes \rho_0$ on decoherence timescales, one can derive the following Lindblad master equation for the center of mass dynamics:

$$\dot{\rho}_{\rm cm} = -\frac{i}{\hbar}\left[H_{\rm cm}, \rho_{\rm cm}(t)\right] - \kappa t\left[X, \left[X, \rho_{\rm cm}(t)\right]\right], \tag{2.17}$$

$$\kappa \equiv \left(\frac{\hbar}{m\omega_0}\right)\left(\frac{\Delta E_0 g}{\hbar c^2}\right)^2, \tag{2.18}$$

$$\Delta E_0 \equiv \sqrt{\langle H_0^2\rangle - \langle H_0\rangle^2}. \tag{2.19}$$

The form of Eq. (2.17) ensures always divisible and hence Markovian dynamics [44] and is a special case of the interaction picture quantum Brow-

nian motion master equation:

$$\begin{aligned}\frac{d\rho(t)}{dt} =& -\Delta_B(t)\,[X,[X,\rho(t)]] + \Pi_B(t)\,[X,[P,\rho(t)]] \\ &+ \frac{i}{2}R_B(t)\left[X^2,\rho(t)\right] - i\Gamma_B(t)\,[X,\{P,\rho(t)\}]\end{aligned} \tag{2.20}$$

for $\Pi_B(t) = R_B(t) = \Gamma_B(t) = 0$ and $\Delta_B(t) = \kappa t$. This allows us to use the general solution of the quantum Brownian motion model from Refs. [45–48]:

$$\rho_{\rm cm}(t) = \frac{1}{2\pi}\int d\xi d\xi^* \chi(\xi,t) D(\xi),\ \xi \in \mathbb{C}. \tag{2.21}$$

The solution uses the symmetrically ordered quantum characteristic function, to be generalized in the next section,

$$\begin{aligned}\chi(\xi,t) =& \chi(\xi,0)e^{-N(t)|\xi|^2}, \\ N(t) =& \tfrac{1}{2}\kappa t^2 = \textstyle\int_0^t dt' \Delta_B(t')\end{aligned} \tag{2.22}$$

and the displacement operator

$$D(\xi) = e^{\xi a^\dagger - \xi^* a}, \tag{2.23}$$

called so as it can be used to displace localized states by a magnitude ξ. For ladder operators $a^\dagger$ and a, the displacement operator satisfies

$$\begin{aligned}D^\dagger(\xi) a D(\xi) =& \ a + \xi I, \\ D(\xi) a D^\dagger(\xi) =& \ a - \xi I.\end{aligned} \tag{2.24}$$

2.3 Decoherence dynamics

The above solution enables us to determine the evolution of a particular initial state. Contrary to Ref. [4], we shall consider the initial state to be the Schrödinger cat state, or specifically the even coherent state [49] here restricted to $\alpha \in \mathbb{R}$ for simplicity:

$$\begin{aligned}\rho_{\rm cm}(0) =& \ |\Psi\rangle\langle\Psi|, \\ |\Psi\rangle =& \ \tfrac{1}{\sqrt{\mathcal{N}}}(|\alpha\rangle + |-\alpha\rangle).\end{aligned} \tag{2.25}$$

The normalization factor is $\mathcal{N} = \frac{1}{2}\left(1 + e^{-2|\alpha|^2}\right)^{-1}$ and $|\alpha\rangle$ is a coherent state of a quantum harmonic oscillator, first proposed by E. Schrödinger [50] and obtained by operating on the q.h.o. ground state with the displacement operator (2.23):

$$|\alpha\rangle = D(\alpha)|0\rangle.$$

The *size* of the cat state is now given by $\Delta x = 2\alpha\Delta x_0$, with Δx_0 from Eq. (2.15), and 2α the distance between the peaks of the two Gaussian functions describing, in phase space, the coherent state components of the superposition.

To study the time evolution of the state in Eq. (2.25), we need to define the family of s-ordered characteristic functions $\chi_s(\xi)$ and their Fourier transforms, the family of quasi-probability distributions $W_s(\alpha)$:

$$\chi_s(\xi) = \mathrm{Tr}[\rho D(\xi)]e^{\frac{1}{2}s|\xi|^2}, \tag{2.26}$$

$$W_s(\alpha) = \frac{1}{\pi^2}\int d\xi d\xi^* e^{\alpha\xi^* - \alpha^*\xi}\chi_s(\xi). \tag{2.27}$$

$W_s(\alpha)$ is not a true probability distribution as it is allowed to take negative values for $\forall s > -1$. The function $W_s(\alpha)$ defines the Well-known Wigner, Glauber (or P) and Husimi (or Q) functions for $s = 0, 1$, and -1, respectively, while $\chi_s(\xi)$ corresponds to the symmetrically, normally and antinormally ordered characteristic functions for the aforementioned values of s. For now we shall only need the Wigner function and hence will be omitting the subscript $s = 0$ for brevity further in this section.

The above description enables us to write the dynamics of the Wigner function for the initial state (2.25) by singling out the terms describing two Gaussian peaks as well as the quantumness-characterizing interference term as follows [48]:

$$W(\beta, t) = W^{+\alpha}(\beta, t) + W^{-\alpha}(\beta, t) + W_I(\beta, t), \tag{2.28}$$

where

$$W^{\pm\alpha}(\beta, t) = \frac{\mathcal{N}}{\pi\sqrt{N(t) + 1/4}} e^{-\frac{\mathrm{Im}(\beta)^2}{2N(t)+1/2}} e^{-2(\mathrm{Re}\beta \mp \alpha)^2} \tag{2.29}$$

and

$$W_I(\beta,t) = \frac{\mathcal{N}}{\pi\sqrt{N(t)+1/4}}\cos\left(\frac{1}{N(t)+1/4}\alpha\mathrm{Im}\beta\right) \times e^{-2\alpha^2\left(1-\frac{1}{4N(t)+1}\right)} e^{-\frac{\mathrm{Im}(\beta)^2}{2N(t)+1/2}-2\mathrm{Re}(\beta)^2}. \tag{2.30}$$

As decoherence occurs, the term of Eq. (2.30) decays with a characteristic decoherence time. We now use the values of peaks of the Wigner function components in Eq. (2.28) to introduce the fringe visibility function as per the standard description of environment-induced decoherence [45–48, 51]

$$F(\alpha,t) = \frac{1}{2}\frac{W_I(\beta=(0,0),t)}{\sqrt{W^{+\alpha}(\beta=+\alpha,t)W^{\alpha}(\beta=-\alpha,t)}} \tag{2.31}$$

$$= e^{-2\alpha^2\left(1-\frac{1}{1+4N(t)}\right)}. \tag{2.32}$$

The fringe visibility function measures the peak-to-peak ratio between the Gaussian and the interference components. In the limit of $\kappa t^2 \ll 1$, we can simplify Eq. (2.32) to

$$F(\alpha,t) \approx e^{-2\alpha^2\kappa t^2} \equiv e^{-(t/\tau_{\mathrm{dec}})^2}, \tag{2.33}$$

$$\tau_{\mathrm{dec}}^2 = (4\alpha^2\kappa)^{-1}. \tag{2.34}$$

Equation (2.33) is valid only for $t \ll \tau_{\mathrm{dec}}\frac{\Delta x}{\Delta x_0}$ since generally $\frac{\Delta x}{\Delta x_0} > 1$, i.e. the separation between the two components of the superposition is larger than their respective width. In the above description, we assume that both the observer and the system are at approximately the same finite distance from the source of gravity, $r_{\mathrm{sys}} \approx r_{\mathrm{obs}}$, as in most experimental settings, the observer and the system are located in the same laboratory. One can however, picture a situation where the observer and the laboratory housing the system are separated by a large distance. This situation requires gravitational time-dilation corrections described in Sec. 2.1, presenting us with the following relation between rest frames of the observer and the system:

$$-\left(1-\frac{r_s}{r_{\mathrm{sys}}}\right)^{-1} dt_{\mathrm{sys}}^2 = -\left(1-\frac{r_s}{r_{\mathrm{obs}}}\right)^{-1} dt_{\mathrm{obs}}^2. \tag{2.35}$$

Defining

$$a_{\text{sys(obs)}} = \sqrt{1 - \frac{r_s}{r_{\text{sys(obs)}}}}, \tag{2.36}$$

we can write the decoherence time measured in the observer's rest frame with respect to the decoherence time in the system's rest frame:

$$\tau_{\text{dec}}^{\text{obs}} = \frac{a_{\text{obs}}}{a_{\text{sys}}} \tau_{\text{dec}}^{\text{sys}}. \tag{2.37}$$

The correction $\left(\tau_{\text{dec}}^{\text{obs}} - \tau_{\text{dec}}^{\text{sys}}\right)/\tau_{\text{dec}}^{\text{obs}}$ depends directly on the Schwarzschild radius r_s and is extremely minute for an Earth-like object, at most its order of magnitude is 10^{-13}. However, this relativistic effect is much more pronounced at the vicinity of a heavy stellar object such as a neutron star, with order of magnitude 1 and tending to infinity when approaching the event horizon of a black hole.

2.4 Nonclassicality indicators

The definition of nonclassicality in Eq. (2.31) is not unique and may not fully encompass every aspect of quantumness of a particular state. It is therefore important to explore multiple witnesses of quantum to classical transition. The nonclassicality indicators we use to quantify quantumness in this thesis are among the most widespread ones and are described in Table (2.1). The first two criteria, nonclassical depth and negativity of the Wigner function are of great interest theoretically, but are experimentally demanding as they require full tomography of the state over the course of its evolution. The Vogel and Klyshko criteria, on the other hand, are more experimentally friendly. Vogel criterion can be directly measured through balanced homodyne detection using optical intereferometry and Klyshko criterion is a measure based on phonon counting.

Nonclassicality indicator	Description
Fringe visibility	Ratio of maxima of the interference fringe and the two Gaussian components of the Wigner function [5]
Nonclassical depth	The minimum number of thermal photons required to destroy any non-classical characteristics of the system [6]
Negativity of the Wigner function	Measures the separation between the Wigner quasiprobability distribution and a classical probability distribution [7]
Vogel criterion	Quantifies nonclassicality by measuring the decay rates of the characteristic function of the quadrature distributions or the s-parametrized phase-space distributions [8]
Klyshko criteron	Compares classical and quantum phonon number probability distributions [9]

Table 2.1: Table of nonclassicality indicators

2.4.1 Nonclassical depth

The nonclassical depth is defined through the supremum of a generalized (continuous in s) quasiprobability distribution as

$$\eta = \frac{1}{2}(1 - \bar{s}), \tag{2.38}$$

$$\bar{s} = \sup\{s \in [-1, 1] | W_s(\alpha) \leq 0\}, \tag{2.39}$$

where $W_s(\alpha)$ is defined in Eq. (2.27). We can rewrite $W_s(\alpha)$ as a convolution

$$W_s(\alpha) = W_{s'}(\alpha) \star G(s'-s,\alpha) \tag{2.40}$$

$$= \int d^2\beta\, W_{s'}(\beta)\, G(s'-s,\alpha-\beta), \tag{2.41}$$

$$G(s'-s,\alpha) = \frac{2}{\pi(s'-s)} e^{-2\frac{|\alpha|^2}{s'-s}}. \tag{2.42}$$

Setting $s'=1$ in Eq. (2.40) and noticing that for the Fourier transform of a product of functions, $\mathcal{F}\{f\cdot g\} = \mathcal{F}\{f\} \star \mathcal{F}\{g\}$, we obtain the convolution in the form of the P-function:

$$W_s(\alpha) = P(\alpha) \star G(1-s,\alpha). \tag{2.43}$$

We can now use Eq. (2.22) to obtain the time-dependent P-function

$$\begin{aligned} P(\alpha,t) &= \tfrac{1}{\pi}\textstyle\int d\xi^2 \chi_0(\xi) e^{-N(t)|\xi|^2+\alpha\xi^*-\alpha^*\xi} \\ &= P(\alpha,0)\star G(1-s(t),\alpha) \\ &= W_{s(t)}(\alpha), \\ s(t) &= 1-2N(t). \end{aligned} \tag{2.44}$$

This shows that the initial P-function is transformed into other characteristic functions by the dynamics of the system. In particular, one can prove [52] that at time τ_p, it is transformed into the Q-function, which is always positive and hence a regular classical probability distribution. The time τ_p can be solved from Eq. (2.44):

$$s(\tau_p) \equiv 1-2N(\tau_p) = -1 \tag{2.45}$$

$$\Rightarrow \tau_p^2 = 2/\kappa. \tag{2.46}$$

The form of the decoherence time in Eq. (2.46) is independent of the size of the superposition α and is directly related to the decoherence time for the fringe visibility in Eq. (2.34) by $\tau_p = 2\alpha\tau_{\mathrm{dec}}$.

2.4.2 Negativity of the Wigner function

The negativity of the Wigner function is related to the nonclassical depth, as one can see once again using the convolutional form of the Wigner function in Eq. (2.40). The Wigner function of the initial cat state (2.25) has regions of negativity and we are interested in identifying the time τ_W after which the Wigner function is positive everywhere. This can be calculated by solving for s_{τ_W} as follows

$$\begin{aligned} s_{\tau_W} &= 1 - 2\kappa\tau_W^2 = 0 \\ \Rightarrow \tau_W^2 &= 1/\kappa. \end{aligned} \tag{2.47}$$

As $\tau_W^2 = \tau_p^2/2$, the negativity of the Wigner function vanishes quicker than nonclassicality measured by the nonclassical depth and notably does not depend on the size α.

2.4.3 Vogel criterion

Nonclassicality of state defined through the Vogel criterion is related to its normally ordered characteristic function, the state is considered nonclassical at time t iff

$$\exists u, v \in \mathbb{R} \text{ s.t. } |\chi_1(\xi, t)| > 1, \text{ with } \xi = u + iv, \tag{2.48}$$

which for our solution in Eq. (2.22) leads to

$$\chi_1(\xi, t) = \chi_1(\xi, 0) e^{-N(t)|\xi|^2}. \tag{2.49}$$

Using the expression of $\chi_1(\xi, 0)$ for the initial Schrödinger cat state we can write the criteria $\chi_1(\xi, t) = \chi_1(u, v, t) > 1$ as follows

$$\begin{aligned} \chi_1(u, v, t) &= \tfrac{2}{\mathcal{N}} e^{-N(t)(u^2+v^2)} \left[\cos(2\alpha v) + e^{-2\alpha} \cosh(2\alpha u)\right] \\ &\leq \chi_1(u, 0, t). \end{aligned} \tag{2.50}$$

In general, the criterion in question depends on the state and in our case it depends specifically on the size parameter α. The decoherence time τ_V can be obtained numerically from the condition $\chi_1(u, 0, \tau_V) = 1$. In the limit $\alpha \to \infty$ however, the condition $2N(\tau_V) \leq 1$ analytically leads to an upper

bound of the onset of classicality

$$\tau_V^2 = 1/\kappa, \tag{2.51}$$

which is equivalent to the negativity of the Wigner function.

2.4.4 Klyshko criterion

The Klyshko criterion is well suited for experimental settings as it only requires measurements of phonon number distributions $p(n) = \langle n|\rho|n\rangle$. The sufficient condition for nonclassical phonon counting statistics in this criterion is [9, 46, 53]

$$\exists n \in \mathbb{N} \text{ s.t. } (n+2)p(n)p(n+2) - (n+1)(p(n+1))^2 < 0. \tag{2.52}$$

The function $p(n)$ can be written in terms of the time-dependent $s = 1$ and phonon number-dependent $s = -1$ characteristic functions, where the latter takes the form $\chi_{-1}(u, v, n) = e^{-u^2-v^2} L_n(u^2)$, with Laguerre polynomials $L_n(x)$. The exact form of the time-dependent phonon number probabilities is

$$p(n,t) = \frac{1}{\pi} \int_0^\infty \int_0^\infty dudv \chi_1(u, v, t) e^{-u^2-v^2} L_n(u^2), \tag{2.53}$$

and to find the time τ_K at which the function in Eq. (2.52) is exactly $= 0$ requires numerical analysis.

The numerical results and cross-comparisons of decoherence rates according to the nonclassicality indicators used are presented in Fig. (2.1). It is worth noting that the corresponding decoherence rates obey a general order $\tau_K < \tau_V < \tau_W < \tau_p$ for all α and $\tau_{\text{dec}} < \tau_K$ for $\alpha > 1$.

2.5 Gravitational decoherence vs classical noise

A potential interferometric experiment with the goal of measuring the effect of gravitational decoherence on a quantum system will always be affected by general classical measurement noise which also destroys decoherence and may therefore hide the time dilational induced effect. Some analysis of competing decoherence effects has been performed in Ref. [54], however if we consider classical stochastic noise, it is possible to perform a numerical ex-

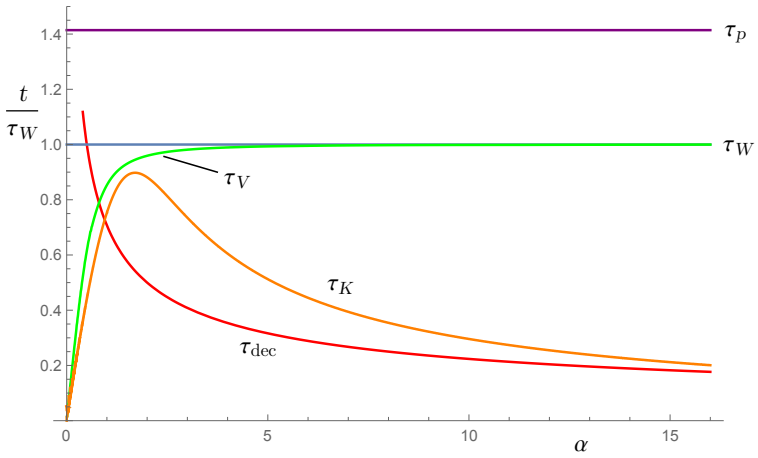

Figure 2.1: Decoherence rates of various nonclassicality indicators plotted as a function of the size parameter α and scaled by the α-independent indicator τ_W.

act analysis without invoking the Born-Markov approximations commonly done for quantum environments. This would extend the observability of gravitational decoherence to situations with significant memory effects and is achievable by, e.g., reservoir engineering, which allows manipulation of environment in order to achieve longer coherence times.

We follow the results of Ref. [52] and examine a quantum harmonic oscillator subjected to a classical stochastic field, described by the Hamiltonian

$$H_{SC} = \hbar \left(a\bar{B}(t)e^{i\omega t} + a^\dagger B(t)e^{-i\omega t} \right), \tag{2.54}$$

where $B(t) = B_x(t) + iB_y(t)$ is a function of a Gaussian stochastic process with the following averages over all stochastic realizations

$$\begin{aligned} \langle B_x(t)\rangle_B &= \langle B_y(t)\rangle_B = 0, \\ \langle B_x(t_1)B_x(t_2)\rangle_B &= \langle B_y(t_1)B_y(t_2)\rangle_B = K(t_1,t_2), \\ \langle B_x(t_1)B_y(t_2)\rangle_B &= \langle B_y(t_1)B_x(t_2)\rangle_B = 0. \end{aligned} \tag{2.55}$$

The $K(t_1, t_2)$ is the kernel autocorrelation function which we choose to

represent the Ornstein-Uhlenbeck process as per Ref. [55]:

$$K(t_1, t_2) = \frac{1}{2}\lambda\gamma e^{-\gamma|t_1 - t_2|}, \tag{2.56}$$

The evolved state can be written in terms of the s-ordered characteristic functions as

$$\begin{aligned} \chi_s(\xi) &= \chi_s(\xi, 0) e^{\frac{1}{2}|\xi|^2(s-2\sigma(t))}, \\ \sigma(t) &= \int_0^t \int_0^t ds_1 ds_2 \cos\left[\delta(s_1 - s_2)\right] K(s_1, s_2), \end{aligned} \tag{2.57}$$

where $\sigma(t)$ has a simple expression for resonant interaction and the process considered here [52]:

$$\sigma(t) = \lambda t + \frac{\lambda}{\gamma}\left(e^{-\gamma t} - 1\right). \tag{2.58}$$

The parameters λ and γ represent the system-noise coupling constant and the temporal correlations of the environment, respectively. The inverse of γ can be thought of as the memory time of the environment. Comparison of Eqs. (2.22) and (2.57) shows the similarity of the forms of the quantum characteristic functions describing the time evolution in presence of classical stochastic noise and the one describing time dilation induced decoherence.

The Vogel and Klyshko criteria can be studied in the same manner as in section (2.4). For the negativity of the Wigner function and the nonclassical depth (related to each other by $\tau_p^2 = 2\tau_W^2$), we can calculate a direct form of the decoherence time due to classical noise:

$$\tau_W(\gamma, \lambda) = \omega_0 \left[\frac{\gamma + 2\lambda}{2\gamma\lambda} + \frac{1}{\gamma}\text{ProductLog}\left(-e^{1-\frac{\gamma}{2\lambda}}\right)\right]. \tag{2.59}$$

In Fig. 2.2, we can see the benchmark of various gravitational decoherence rates against decoherence induced by classical noise as a function of values λ and γ as a ratio between the gravitational and classical noise decoherence rates evaluated by corresponding nonclassicality measures. The darkened portion of the plot depicts the range where classical noise overwhelms the gravitationally induced one. It is generally very difficult to estimate the values of parameters for realistic experiments. In Ref. [55] however, the authors present one of the most precise examples of a trapped Scrödinger cat state in the form of an atom and indicate the value of γ to

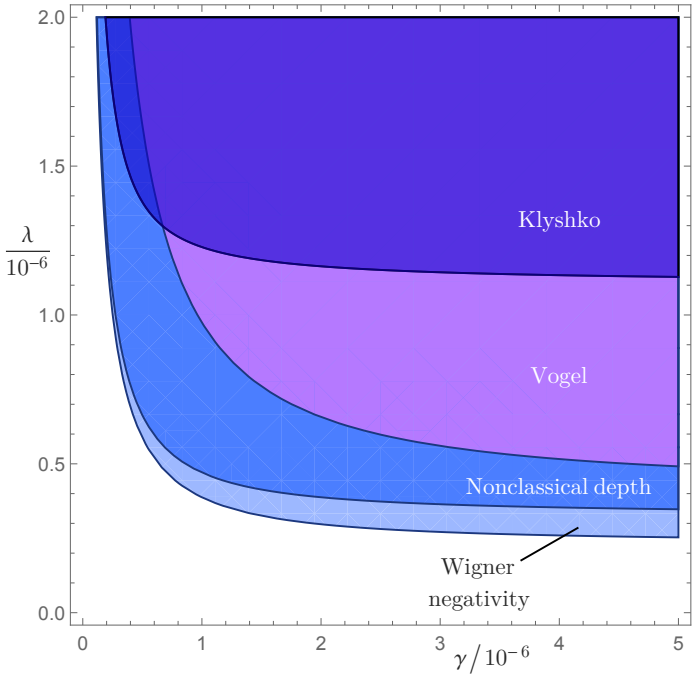

Figure 2.2: Ratio between the decoherence times for different nonclassicality indicators due to classical noise and those due to time dilation induced decoherence, as a function of γ and λ for $\alpha = \sqrt{2}$. The shaded areas represent the region of parameters in which decoherence due to classical noise dominates over time dilation induced decoherence. γ and λ are given in units of ω_0 (Hz).

be, in our units, on the order of 10^{-3}. Modern experiments are therefore still lacking in precision to be successfully detect gravitationally induced decoherence.

Chapter 3

Unruh effect

In this chapter, we will apply the formalism of open quantum systems to a paradigmatic relativistic effect, namely the Unruh effect. Quantum field theory predicts that a detector accelerating in empty Minkowski space shall observe a particle bath with a spectrum dependent on the proper acceleration of the detector. In particular, if the motion is linear with constant proper acceleration, the particle bath is thermal with a temperature proportional to the acceleration of the detector [56, 57]. This extremely minute physical phenomenon is called the Unruh effect. Our aim is to go beyond the usually performed approximations and explore memory effects in terms of information flow in this system.

The last few years have witnessed a tremendous advancement in the theoretical description, as well as in the physical understanding, of open quantum systems beyond the Markovian approximation. This progress has been made possible by the introduction of concepts and tools of quantum information theory for the description of open quantum systems. This has led to a deeper physical understanding of memory effects and non-Markovianity in terms of information flow and information exchange between system and environment. At the same time, it has spurred several investigations on the possibility of using such memory effects for improving the efficiency of quantum technologies and devices.

The results we summarize in this chapter, presented in paper (III), are the first attempt to bridge another gap between two scientific fields which have not been communicating much until now. Specifically, open quantum system dynamics (and in particular the modern understanding and description of non-Markovianity) and relativistic quantum field theory.

In this spirit, we revisit the Unruh effect and show that, when releasing two previously done restricting assumptions, the master equation describing

the dynamics of an accelerated detector interacting with Minkowski vacuum is in fact non-Markovian.

Interestingly, we identify the physical parameter, connected to the detector's properties such as its internal energy and its acceleration, responsible for the appearance of information back flow and memory effects. In so doing, we demonstrate that the modern approaches to non-Markovianity and, in general non-equilibrium quantum dynamics, allow us to gain new insight and are useful also in relativistic quantum field theory.

We believe that cross-fertilization between these two fields may pave the way to a better understanding of a number of open problems in relativistic quantum field theory by introducing new tools, approaches and perspectives.

3.1 The physics of the Unruh effect

In 1976 William Unruh demonstrated theoretically [56] that an observer's notion of particle vacuum depends on the observer's worldline through spacetime. More specifically, the observed positive frequency modes of the quantum field with which the observer is interacting depend directly on the inertiality of the observer. This can be shown by constructing a comoving coordinate frame of the accelerated observer and comparing the solutions of the wave equation of the inertial and accelerated frames [58].

An observer moving along axis x^1 with uniform proper acceleration $a_p = \alpha^{-1}$ through Minkowski spacetime has the following trajectory (see Fig. (3.1)).

$$\begin{aligned} x^0(\tau) &= \alpha \sinh\left(\frac{\tau}{\alpha}\right), \\ x^1(\tau) &= \alpha \cosh\left(\frac{\tau}{\alpha}\right), \\ x^2(\tau) &= 0 = x^3(\tau). \end{aligned} \tag{3.1}$$

We can then switch to the non-inertial coordinates of the observer and derive the following locally flat line element in Rindler coordinates (ξ^0, ξ^1):

$$ds^2 = e^{2a\xi^1}\left[(d\xi^0)^2 - (d\xi^1)^2\right]. \tag{3.2}$$

The Rindler coordinates are related to Minkowski coordinates by[58]:

$$\begin{aligned} x^0(\xi^0,\xi^1) &= a_p^{-1} e^{a_p \xi^1} \sinh(a_p \xi^0), \\ x^1(\xi^0,\xi^1) &= a_p^{-1} e^{a_p \xi^1} \cosh(a_p \xi^0). \end{aligned} \tag{3.3}$$

While an inertial observer defines the positive frequency modes using the Minkowski time t, the accelerated observer has to use the proper time $\tau = \xi^0$. The discretized scalar field with which the observer interacts can in general be expanded as [59]

$$\phi(x) = \sum_i [a_i u_i(x) + a_i^\dagger u_i^*(x)]. \tag{3.4}$$

This defines the creation and annihilation operators in spacetimes of certain properties such as ours. In consequence, the positive frequency modes $u_i^*(x)$ of the vacuum scalar field with respect to t appear as superpositions of positive and negative frequency modes with respect to ξ^0 [58].

The definition of a Minkowski vacuum state $|0\rangle^M$ can be postulated as the state which is the eigenstate of the annihilation operator a^M:

$$a^M |0\rangle^M = 0. \tag{3.5}$$

Therefore, in volume V, the expectation value of the particle number operator $n^M = (a^M)^\dagger a^M$ / V would be 0:

$${}^M\langle 0|n^M|0\rangle^M = 0. \tag{3.6}$$

However, the same particle number operator in Rindler coordinates n^R would have a nonzero expected particle number. Specifically, the following form is recovered for frequency Ω [58],

$${}^M\langle 0|n_\Omega^R|0\rangle^M = \left(e^{\frac{2\pi\Omega}{a_p}} - 1\right)^{-1}. \tag{3.7}$$

As this is the direct form of the Bose-Einstein distribution, from the viewpoint of the accelerated observer, the vacuum of an inertial observer appears to be a state containing a thermal equilibrium of particles i.e., a thermal

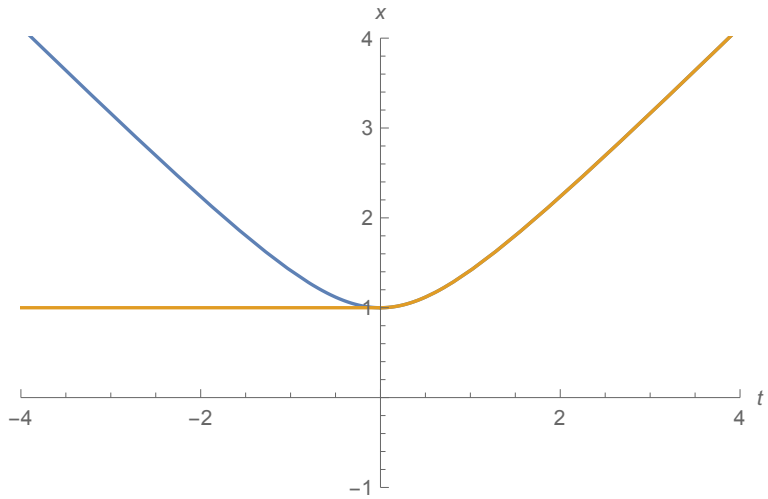

Figure 3.1: Behavior of different paths, blue with eternal constant acceleration $\alpha = 1$, yellow with $\alpha = 0$ for $\tau < 0$ and $\alpha = 1$ for $\tau > 0$.

bath at temperature T_U:

$$k_{\mathrm{B}} T_U = \frac{a_p}{2\pi}, \tag{3.8}$$

where k_B is the Boltzmann constant.

In other words, while the accelerated detector undergoes emission and absorption due to its interaction with a thermal bath, an inertial detector will only experience spontaneous emission or, if it is in the ground state, will not interact with the field at all. Indeed, more elaborate calculations on the system show that the energy momentum tensor describing the particle content of the space vanishes in any coordinate system, and in particular in the inertial as well as in the rest frame of the accelerated detector [59]. This simply means that the particles detected by the accelerated detector are not real but rather *fictitious* particles.

The source of energy for the excitation of the accelerating detector is, indeed, its direct coupling to the surrounding vacuum field [57, 59, 60]. As the detector accelerates, it feels resistance and work is done on it by the external system. The work done not only accelerates the detector but also excites it: to overcome the resistance it is converted into the thermal

field affecting the non-inertial detector. Thus the energy is not provided by any external particle field but rather originates from the unspecified force keeping the detector in the state of accelerating motion.

3.2 Unruh effect: the master equation

In 2004 F. Benatti and R. Floreanini microscopically derived the master equation describing the dynamics of a two-level detector weakly interacting with a scalar field in the Minkowski vacuum [10]. The derivation relies on the standard Born-Markov approximation [30]. An eternally and uniformly accelerated detector parametrized with the proper time, i.e., following the well known hyperbolic path [56], is considered by the authors. Here we relax this unrealistic assumption and consider instead a different trajectory in Minkowski space, assuming that the detector is inertial until a certain time after which it experiences a uniform acceleration, see Fig. (3.1). Under these conditions the environment correlation function is not time-translation invariant anymore, hence Eq. (1.20) does not hold and this leads to decay rates which are now time dependent. Moreover, following the work of [61], we generalize the description of the detector from point-like, to finite size. We show in paper (III) that with these generalizations, following the same lines of Sec. 1.3, where $\phi(x)$ is now a scalar field of the vacuum, the master equation describing the dynamics of the detector takes the form $\dot{\rho} = -i[H_{\text{eff}}, \rho] + \mathcal{L}(\rho)$, where the dissipator $\mathcal{L}$, in the instantaneous rest frame of the detector, is given by

$$\mathcal{L}(\rho) = \frac{\gamma_1(\tau)}{2} L_1(\rho) + \frac{\gamma_2(\tau)}{2} L_2(\rho) + \frac{\gamma_3(\tau)}{2} L_3(\rho), \tag{3.9}$$

and where the effective Hamiltonian is $H_{\text{eff}} = \omega\sigma_z/2 + \Omega(\tau)$, with $\Omega(\tau)$ a generally time-dependent renormalized frequency. The dissipator is given by the sum of three terms, $L_i(\rho)$, describing, in order, heating, dissipation and dephasing, and having the following form

$$\begin{aligned} L_1(\rho) &= \sigma_+ \rho \sigma_- - \tfrac{1}{2}\{\sigma_-\sigma_+, \rho\} \\ L_2(\rho) &= \sigma_- \rho \sigma_+ - \tfrac{1}{2}\{\sigma_+\sigma_-, \rho\} \\ L_3(\rho) &= \sigma_z \rho \sigma_z - \rho. \end{aligned} \tag{3.10}$$

We immediately recognize Eqs. (3.9) and (3.10) to be of the phase-covariant form described in Sec. (1.3). The coefficients $\gamma_1(\tau)$, $\gamma_2(\tau)$ and $\gamma_3(\tau)$ are the absorption, emission and dephasing rates, respectively, with the implicit ω dependence. They are simply related to the proper time $(\tau-)$derivative of the correlation function $F_\tau(\omega)$ through the equations

$$\gamma_1(\tau) = 4\dot{F}_\tau(-\omega),\ \gamma_2(\tau) = 4\dot{F}_\tau(\omega),\ \gamma_3(\tau) = 2\dot{F}_\tau(0). \tag{3.11}$$

For any detector the correlation function is related to the Wightman function $W(\tau,\tau') = \langle\phi(x(\tau))\phi(x(\tau'))\rangle$ on detector worldline $x(\tau)$ as follows [59]:

$$F_\tau(\omega) = \int_{\tau_0}^{\tau} d\tau' \int_{\tau_0}^{\tau} d\tau'' e^{-i\omega(\tau'-\tau'')} W(\tau',\tau''), \tag{3.12}$$

Hence, the proper time derivative $\dot{F}_\tau(\omega)$, for an always-on detector, i.e., for $\tau_0 \to -\infty$, in its rest frame, reads as

$$\dot{F}_\tau(\omega) = 2\int_0^\infty ds \mathrm{Re}\left(e^{-i\omega s} W(\tau,\tau-s)\right). \tag{3.13}$$

Contrarily to the Benatti and Floreanini master equation, our system is governed by a time-local master equation with time-dependent decay rates which may take temporarily negative values. This time-local structure highlights the departure from the Markovian semigroup dynamics described by the well-known GKSL master equation. Note that the time-dependent decay rates are always directly dependent on the detector's trajectory, which in our case is different from the standard eternally accelerated case. We also stress that we use a modified Wightman function to take into account the detector's profile, as proposed in Ref. [61].

The explicit calculation of the time-dependent coefficients leads to the following equation:

$$\begin{aligned} 2\pi\alpha\dot{F}_{\bar{\tau}}(\bar{\omega}) =& \frac{\bar{\omega}}{e^{2\pi\bar{\omega}}-1} + \Delta\dot{F}_{\bar{\tau}}(\bar{\omega}), \\ \Delta\dot{F}_{\bar{\tau}}(\bar{\omega}) \equiv& \frac{1}{\pi}\int_{\bar{\tau}}^\infty \mathrm{d}\bar{s}\cos(\bar{\omega}\bar{s})\left(\frac{1}{(\Delta\mathtt{x})^2_>} - \frac{1}{(\Delta\mathtt{x})^2_<}\right), \end{aligned} \tag{3.14}$$

where

$$(\Delta \mathtt{x})^2_{>} := -\left(\sinh(\bar{\tau}) - (\bar{\tau} - \bar{s})\right)^2 + \left(\cosh(\bar{\tau}) - 1\right)^2$$
$$(\Delta \mathtt{x})^2_{<} := -4\sinh^2(\bar{s}/2), \tag{3.15}$$

with $\bar{\omega} = \omega\alpha$, $\bar{\tau} = \frac{\tau}{\alpha}$ and $\bar{s} = \frac{s}{\alpha}$.

For negative times $\bar{\tau} < 0$ the rate of an inertial detector, $\dot{F}_{\bar{\tau}}(\bar{\omega}) = -\frac{\omega}{2\pi}\theta(-\omega)$, is restored reflecting the fact that only emission can happen. For positive times $\bar{\tau} > 0$ the transition rate is the sum of the Planckian equilibrium part $\bar{\omega}/(e^{2\pi\bar{\omega}} - 1)$ and a dynamical correction $\Delta\dot{F}_{\bar{\tau}}(\bar{\omega})$ which tends to zero in the asymptotic limit $\bar{\tau} \to \infty$. In this limit we obtain the same GKSL master equation as in Ref. [10].

3.3 Information backflow and non-Markovianity

We note that the behavior of the decay rates crucially depends on the α-multiplied angular frequency $\bar{\omega}$, and hence on both the detector energy $\hbar\omega$ and the proper acceleration; in particular, for fixed ω, larger values of $\bar{\omega}$ correspond to smaller proper acceleration, i.e. smaller deviation from the inertial system. Also, since the proper acceleration is proportional to the effective Unruh temperature T_U, $\bar{\omega}$ can be seen as the ratio between the detector energy and the effective bath thermal energy $k_B T_U$. We will see that this parameter drives the transition between Markovian and non-Markovian dynamics in the Unruh effect.

We recall that, if at least one of the coefficients becomes negative at some time, then the dynamical map is not CP divisible and therefore information flows back into the system-ancilla pair as discussed in Sec. 1.5 in the framework of the generalization of BLP non-Markovianity. However, the system can still be BLP Markovian, meaning that there is no information backflow into the system only, but information does return to a larger Hilbert space which includes an ancilla.

The dephasing rate can be calculated explicitly and has the form

$$\pi\alpha\gamma_3(\bar{\tau}) = \frac{1}{2\pi}\frac{\bar{\tau} - \sinh(\bar{\tau})}{1 - \cosh(\bar{\tau})}. \tag{3.16}$$

From this equation we see that $\gamma_3(\bar{\tau})$ is always non-negative for our system. The absorption and emission rates, defined for $\bar{\omega} \neq 0$, require numerical

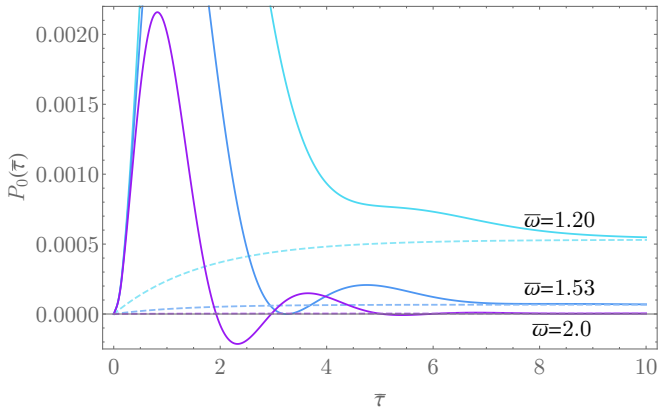

Figure 3.2: The ground state probabilities $P_0(\bar{\tau})$ for $\bar{\omega} = 1.20$ (lightblue), 1.53 (darkblue), 2.0 (violet) starting from top, where $P_0(\bar{\tau}) < 0$ indicates CP violation. Dashed lines represent the Markovian behavior without time-dependent contribution.

approaches. Extensive numerical investigation shows that the absorption rate is positive at all times.

The emission rate $\gamma_2(\bar{\tau})$ displays a more interesting temporal behavior, since it can attain negative values for $\bar{\omega} \geq 1$, as shown in Fig. (3.3). The parameter $\bar{\omega}$, therefore, controls the transition between CP divisibility and CP nondivisibility, with $\bar{\omega} \approx 1$ the transition value. In the intervals of time where $\gamma_2(\bar{\tau})$ is negative the system-ancilla pair experiences information backflow and memory effects. This happens approximately when the detector energy becomes greater than the thermal energy of the effective bath, i.e., for small Unruh temperatures (or small proper accelerations).

In paper (III) we also look at the behavior of other non-Markovianity indicators and show that none of them detect the violation of Markovianity at any value of $\bar{\omega}$. This is consistent with the fact that the quantities considered are only indicators of CP nondivisibility; therefore they may not always detect violation of such property. In other words, in the framework of the system studied, information never returns to the detector only but it will return to a larger system formed by the detector, which interacts with the environment, and an ancilla which does not interact directly with the

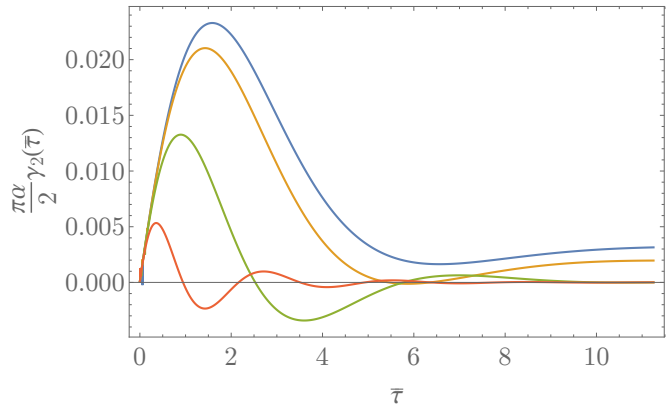

Figure 3.3: Emission rate $\gamma_2(\bar{\tau})$ for $\bar{\omega} = 0.9$ (blue), 1.0 (yellow), 1.6 (green), 4.0 (red) starting from top, showing non-Markovian regions after $\bar{\omega} \approx 1$ threshold.

environment. The ancilla could physically represent, for example, other electronic levels of an atom, if the detector is actually a single atom, or more in general other degrees of freedom which are not explicitly taken into account in the two-state description of the detector and which are not explicitly coupled to the environment.

3.4 Complete positivity

We know that when the decay rates become negative, and hence the dynamics non-Markovian, we cannot rely anymore on the GKSL theorem to guarantee physicality (i.e., complete positivity) of the solution of the master equation. We therefore need to explore the conditions for complete positivity of the time local master equation for the Unruh effect discussed in this Chapter. Using the general result recalled in Chapter 1 and paper (I) we demonstrate that since in our case, $\gamma_3 > 0$ at all times, in our system the complete positivity conditions reduce to the simpler positivity conditions,

given by

$$\begin{aligned} \rho_{11}(\tau) &\equiv e^{-\Gamma(\tau)}\left[G(\tau)+1\right] \in [0,1]\,, \\ \rho_{00}(\tau) &\equiv e^{-\Gamma(\tau)} G(\tau) \in [0,1]\,, \end{aligned} \tag{3.17}$$

where

$$\begin{aligned} \Gamma(\tau) &= \frac{1}{2}\int_0^\tau \mathrm{d}s\,(\gamma_1(s)+\gamma_2(s))\,, \\ G(\tau) &= \frac{1}{2}\int_0^\tau \mathrm{d}s e^{\Gamma(s)}\gamma_2(s). \end{aligned} \tag{3.18}$$

Moreover, $\rho_{11(00)}(\tau)$ can be identified as the ground state probability with initial conditions $\rho_{11(00)}(0)$ equal to 1(0) respectively. The positivity conditions of Eq. (3.17) can be seen as upper and lower bounds to the ground state probability, respectively.

Taking the derivative of Eqs. (3.17) with respect to τ we arrive to a single differential equation, with two different boundary values:

$$\begin{aligned} \rho'_{11(00)}(\tau) &= -\rho_{11(00)}(\tau)\Gamma'(\tau) + \frac{1}{2}\gamma_2(\tau), \\ \rho_{11}(0) &= 1, \\ \rho_{00}(0) &= 0. \end{aligned} \tag{3.19}$$

In Fig. 3.2 we show the dynamics of the ground state probabilities, i.e. functions of the conditions (3.17), for some values of $\bar{\omega}$. Numerical investigations for parameter values $\bar{\omega} > 1.0$, where the decay rate $\gamma_2(\tau)$ already exhibits nonpositivity, reveal that the CP condition is violated, i.e. $\rho_{00}(\bar{\tau}) < 0$, when $\bar{\omega} \gtrsim 1.53$. This indicates the breakdown of the approximations used in the derivation of the master equation for this range of parameters.

Chapter 4

Complex quantum networks

This chapter servers as the introduction of the second half of the thesis. Here we introduce the concept of complex quantum networks in the context of recent literature. A connection between open quantum systems theory and complex quantum networks is discussed in Refs. [62, 63], where it is shown that several types of quantum environments can be engineered by using complex quantum networks. In this case, the networks are quantum systems and links are physical interactions between quantum systems. Here, however, we are interested in a more general setting of which the previous example is just a particular case.

The need to introduce complex quantum networks arises from two main considerations, one related to experiments and another related to computational approaches. Indeed, experiments have been achieving a two-fold feat. On the one hand, they have dramatically increased precision and efficiency of coherent manipulation and measurement of individual quantum systems embedded into large many-body systems. On the other hand, they have been able to perform quantum simulations of such larger systems under very "clean" and controllable conditions [64–69]. Moreover, the increase in (classical) computational power, and the development of efficient algorithms, have enabled to investigate numerically the properties of larger many-body quantum systems [70]. Finally, skillful techniques for tomographic reconstruction of both quantum states and channels have been developed [71, 72], together with a variety of error correction approaches. This means that we are starting to have at our disposal vast experimental and numerical data sets containing an enormous amount of information on the behaviour of quantum many-body systems. A crucial question can be therefore posed: can we use complex network approaches to analyze and extract as much information as possible from these data?

For classical complex systems, the development of complex network theory, consequent and motivated by the availability of big data sets, has not only provided a theoretical framework to analyze emergent phenomena but, most importantly, has permitted to introduce models explaining their origin. Merging and, when needed, generalizing the approaches and mathematical tools of complex network theory and quantum physics amounts to developing the theory of complex quantum networks. Some attempts have been initiated in this direction [73]. Most of the examples studied fall into two categories: networks of entanglement, wherein connections (links) represent entangled states [74–76], and networks of quantum systems where the links are physical interactions [63, 77–85].

Only very recently, however, the idea of using a network representation to describe the properties of complex many-body quantum states has been put forward [86, 87]. The latter is the framework we are interested in. This is also motivated by the development of our pairwise tomography algorithm described in the next chapter, which allows one to construct networks of any pairwise quantity from the reduced two-body density matrix. In the following sections we review the main concepts of classical network theory in order to establish a common language which will be used in the description of quantum many-body systems.

4.1 What are quantum network representations and why to use them?

In this section, we introduce quantum network representations of a many-body quantum state, focusing specifically on N-qubit systems. Renowned examples of such states are quantum spin chains and lattices, which are cornerstone models of condensed matter physics. The properties of the ground states of such systems are characterized through a hierarchy of m-body correlation functions, which in turn can be calculated by means of m-body reduced density operators obtained from the density matrix of the N-spin system by partial trace over the degrees of freedom of the other $N-m$ spins. An efficient technique for performing two-body tomography is presented in paper (IV), making two-body correlators experimentally accessible even for large N.

A great deal of the physics of quantum spin chains can be inferred from the knowledge of two-spin correlation functions such as $\langle \sigma_i^l \sigma_j^m \rangle$, where σ_i^l

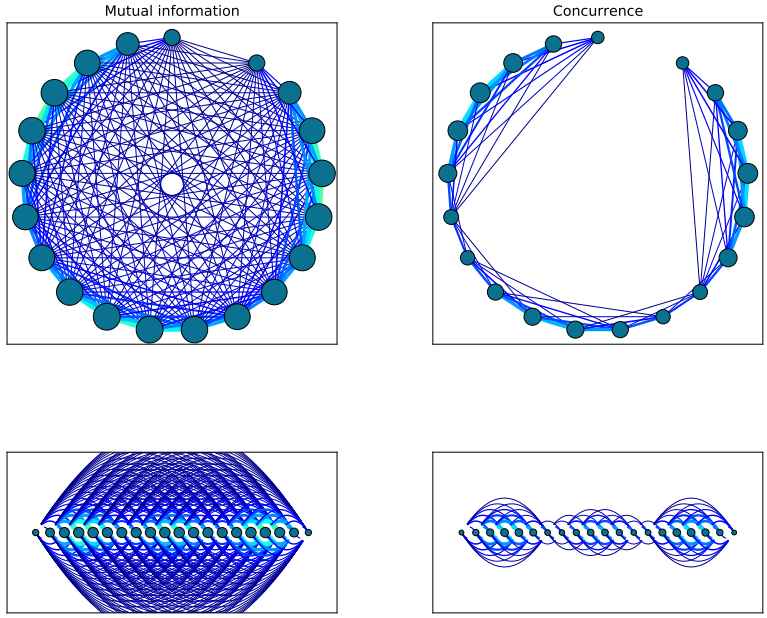

Figure 4.1: Two representations of two networks, circular and linear, of the XX model from chapter 6. Subfigures a) and c) represent a mutual information network and subfigures b) and d) a concurrence network for $N = 20$ and $k = 3$ of the XX model.

and σ_j^m are Pauli operators with $i, j \in \{x, y, z\}$ (l and m are spin indices) [88]. While the set of all two-body correlators does not fully characterise the state of the many-body system, its full knowledge does entail a lot of information, as we will illustrate in what follows.

Limiting our attention to two-body — or pairwise — quantities naturally leads to a network representation of the quantum state wherein the nodes of the network are the spins and the weighted links (i.e., with an associated positive real number) correspond to the numerical value of the pairwise quantity considered, e.g., correlations between spin l and spin m (concurrence, discord, classical correlations, quantum mutual information, etc.) or absolute values of correlation functions $|\langle\sigma_i^l\sigma_j^m\rangle|$ [86, 87]. As an example, in Fig. 4.1, we show two ways of representing the network of mutual information between pairs of spins in the XX model.

For growing N one needs to use statistical approaches and network measures in order to extract useful information from the network, since its graphical representation is not directly informative. A crucial aspect we want to emphasize is that the network representation, say for concreteness the network of pairwise concurrence, contains more information than the collection of the individual values of concurrence among all pairs. In a way we could say that "the total is larger than the sum of the parts". We now introduce some crucial concepts and terminology of complex network theory, which the quantum physics reader may be less familiar with.

4.2 Semantics: what do we mean by complex?

In classical complex network theory the term *complex networks* is generally used to identify networks possessing certain structural properties. Indeed, it was recently discovered that diverse real systems possess network representations which display universal properties [89]. These networks are called *real networks* and their features, such as, e.g., scale-free property, small world property, clustering, etc., are very different from the properties of random (Erdős-Rényi) graphs or regular lattices, which are therefore often not referred to as *complex networks*. Independently from the precise definition of such properties, which is beyond the scope of this thesis, to avoid confusion arising from the use of language belonging to a different scientific community, we stress here that our use of the word *complex* in conjunction with *quantum network* is somewhat broader than the classical case. Specifically, we will generally denote by *complex quantum network* a quantum network whose structure (or topology) is non-trivial, even if the network may have a quasi-regular structure. The examples considered in this paper will clarify the reasoning behind this idea.

Finally, we recall that in complex network theory, the term *topology* refers to the structural properties of the network. Topological properties are those characterizing its underlying graph in terms of direct connections and their weights, wherein the location of the nodes does not depend on geometrical properties, such as their physical distance. It should be noted that, in physics, the world *topological* is often used in a different framework and has a slightly different connotation, for example to describe topological defects or topological excitations.

Degree	$d_i = \sum_{j=1}^{N} a_{ij}$	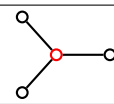
Strength	$s_i = \sum_{j=1}^{N} \omega_{ij}$	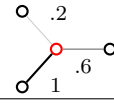
Clustering	$c_i = \frac{\sum_{j,k} a_{ij}a_{ik}a_{jk}}{d_i(d_i-1)}$	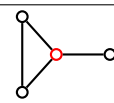
Weighted clustering	$c_i^{\omega} = \frac{\sum_{j,k}(\omega_{ij}\omega_{ik}\omega_{jk})^{1/3}}{d_i(d_i-1)\max_{lm}\omega_{lm}}$	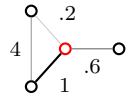
Disparity	$Y_i = \frac{1}{s_i^2}\sum_{j=1}^{N}(\omega_{ij})^2$	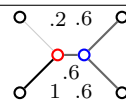

Table 4.1: **Overview of the local network measures used in this paper.** For each measure, we include its definition and a small depiction to illustrate the concept. In the mathematical expressions, ω_{ij} is the weight of the link between nodes i and j (which we identify with the concurrence for our network representation of quantum states), and a_{ij} are the elements of the adjacency matrix of the network, fulfilling $a_{ij} = \Theta(\omega_{ij})$, where $\Theta(x)$ stands for the Heaviside function. Hence, degree and strength account for the number of connections and total weight of a given node, respectively. The red nodes in their respective illustrations have degree $d = 3$ and $s = 1.8$. The clustering coefficient accounts for the fraction of pairs of neighbours of the node that are connected. In the figure, the red node has $c = 1/3$. The weighted version of the clustering used here weights the contribution of each triangle by the geometric mean of the values of the three links involved, normalised by the largest weight in the network, $\max_{lm}\omega_{lm}$; in the example graph, the red node has $c^{\omega} \approx 0.14$. The disparity Y_i quantifies the heterogeneity of the distribution of the weights of the connections of the node. If all its connections have equal weights $\omega_i = s_i/d_i$, $Y_i = 1/d_i$ (as for the blue node). Instead, if one of the links dominates, the disparity approaches 1. For the red node, $Y \approx 0.43$.

4.3 Weighted vs unweighted network properties

A very first distinction we need to consider when introducing quantum network representations is the one between weighted and unweighted networks. For concreteness let us consider entanglement networks. While the unweighted entanglement network gives only binary information on which pairs of spins/nodes are entangled, the weighted network tells also how strongly entangled two spins are, as measured by an entanglement measure

such as concurrence. Hence, weighted networks representations of quantum states contain more information than unweighted ones. Unweighted networks reveal the topological properties of the network representation and it might be useful to compare weighted vs unweighted network measures to identify what these properties are.

It is often the case that for quantum systems with underlying regular geometrical structure, such as spin chains and lattices, the topology of the unweighted quantum state network representation is trivial, except, e.g., in presence of a quantum phase transition. Even if this is the case, the corresponding weighted network may be highly non-trivial and reveal interesting structures in the quantum state of the many-body system.

4.4 Physical meaning of network measures

In this section we introduce a number of network measures and we illustrate their physical meaning. Table 4.1 gives a visual summary of the quantities introduced. As a physical measure, we choose concurrence, which is a measure of entanglement defined for mixed states of two qubits:

$$C(\rho) \equiv \max(0, \lambda_1 - \lambda_2 - \lambda_3 - \lambda_4), \tag{4.1}$$

in which $\lambda_1, ..., \lambda_4$ are the eigenvalues, in decreasing order, of the Hermitian matrix

$$R = \sqrt{\sqrt{\rho}\tilde{\rho}\sqrt{\rho}}, \text{ with} \tag{4.2}$$

$\tilde{\rho} = (\sigma_y \otimes \sigma_y)\rho^*(\sigma_y \otimes \sigma_y)$, where ρ^* is the complex conjugate of ρ and σ_y a Pauli spin matrix. The concurrence ranges from $C = 0$ to $C = 1$ for separable and maximally entangled states, respectively.

4.4.1 Local network measures

- *Node degree*

  In unweighted networks the degree d_i of a node i is the number of nodes connected to it. In entanglement networks the node degree tells how many spins share bipartite entanglement with spin i, and is defined as $d_i = \sum_{j=1}^{N} \Theta(C_{ij})$, where C_{ij} is the concurrence between spin i and spin j, and $\Theta(x)$ the Heaviside step function.

- *Strength*

  The strength s_i generalizes the concept of degree to weighted networks, being the sum of all weights of all links connected to a given node i. In bipartite entanglement networks, this quantity tells not only how many spins are share bipartite entanglement with spin i but also how strong is the bipartite entanglement between spin i and all other spins j to whom it is connected, according to a given entanglement measure. If using concurrence, e.g., we have that $s_i = \sum_{j=1}^{N} C_{ij}$. We note that, differently from the classical case, for entanglement networks the strengths possess an upper bound due to monogamy of entanglement, which therefore imposes constraints on the physically allowed strength distributions.

- *Clustering*

  In network theory the clustering coefficient measures the degree to which nodes in a graph tend to cluster together. The local clustering coefficient, for unweighted networks, is defined as

$$c_i = \frac{1}{d_i(d_i-1)} \sum_{j,k} a_{ij} a_{ik} a_{jk}, \tag{4.3}$$

  with $a_{ij} = 0, 1$ elements of the adjacency matrix, which in this case is the matrix $\{\Theta(C_{ij})\}_{ij}$. For concurrence networks this quantity gives an answer to the following question: what is the probability that two spins entangled with a third one are entangled with one another?

- *Weighted clustering*

  The generalization of the clustering coefficients defined above to weighted networks is straightforward. For concurrence networks, e.g., we have

$$c_i^{\omega} = \frac{\sum_{j,k} (C_{ij} C_{ik} C_{jk})^{1/3}}{d_i(d_i-1) \max_{lm} C_{lm}} \tag{4.4}$$

- *Disparity*

  In a weighted network, the disparity Y_i of node i measures the local heterogeneity of the network at the given site. For concurrence

networks, it is defined as $Y_i = \sum_{j=1}^{N} C_{ij}^2/s_i^2$. If concurrence between all spins takes a constant value, as in the case of W states, then disparity is everywhere constant and given by $Y_i = 1/(N-1)$, i.e., pairwise entanglement is homogeneously distributed among all pairs. If, on the contrary, entanglement between a particular pair (i, j) dominates, then disparity approaches unity and the local distribution is highly heterogeneous.

All the above network measures describe local properties of the network. It is also useful to look at average network measures, obtained by averaging local quantities over all nodes of the network.

4.4.2 Average network measures

- *Density*

  The density D is closely related to the average strength, being defined as $D = \sum_{i=1}^{N} s_i/N(N-1)$. In entanglement networks it quantifies the average pairwise entanglement present in the many-body system.

- *Average disparity*

  The average disparity is straightforwardly defined as $Y = \sum_{i=1}^{N} Y_i/N$ and it indicates how heterogeneously the links, and hence, e.g., pairwise entanglement, are distributed across the spins, on average.

4.4.3 Mesoscopic network structure

The network measures described above are used to reveal local, i.e. microscopic, structures within the network. It is well-known, however, that networks may also possess mesoscopic structures, which are not uncovered at the level of single nodes, reflecting their behaviour as a whole. Examples are the network community structures describing the heterogeneity in the density of links or in the values of the weights within different subsets of the nodes of the network. We call community a subset of nodes with higher density of connection within the subset than with the rest of the network.

Community detection is an important and computationally demanding task in the analysis of complex networks. Many algorithms have been developed and are being developed with the goal of finding the community

structure of large networks quickly and accurately. We use a community detection algorithm, described in paper (V), for analyzing both the weighted and the unweighted entanglement networks.

Chapter 5

Pairwise tomography networks

As the field of quantum technologies progresses, larger and larger quantum systems such as quantum computers and quantum simulators are developed. Despite the clear advantage that such progress represents, not only for the quantum information community, but also for virtually *any* discipline that requires high computational power, working with large quantum systems also poses some dramatic challenges. In particular, one of them is characterizing the quantum state in which the system is at some given time. This task is often crucial both for the verification of the proper functioning of the quantum device and to quantify the outcome of a simulation. The process by which one reconstructs the quantum state is called *quantum state tomography* [90]. However, tomography has the serious drawback of requiring an amount of measurements exponential in the system size, which makes it unfeasible even for relatively small devices. Furthermore, the quantum state of a large number of qubits can be extremely complex, so one might raise the question of how can the relevant information be identified and analyzed from such a large mathematical object.

In this chapter, we summarize the results of paper (IV) wherein this question is addressed by providing a new algorithm to reconstruct all the quantum states of all pairs of qubits very efficiently; as we prove, it only requires an amount of measurement settings logarithmic in the number of qubits. This further enables to construct *complex networks* representing the correlations, both classical and quantum, between the system qubits. This will in turn allow one to borrow valuable techniques from classical network theory, widely used for the understanding of *classical* complex systems, to

the study of *quantum* complex systems.

In order to showcase the potential of our approach in paper (IV), we apply our techniques in several scenarios. First, we show, as a proof-of-principle experiment, that complex networks describing the pairwise entanglement between all the qubits in different IBM Q quantum computers can be efficiently extracted, and that such network representation allows us to identify at a glance the deviations of the devices with respect to their expected behavior. Second, we show that the complexity in the state between the qubits in a dynamical simulation can be conveniently represented in terms of a *multiplex network*, a very well studied mathematical object in the field of network theory; this particular multiplex representation consists of a layered network in which, in every layer, the links represent some relevant quantifier like, e.g., concurrence, quantum discord, entropy, etc. [17, 19, 91]. Finally, the same multiplex description is applied to the study of the ground state of a paradigmatic spin-chain system, the XX model, which reveals rich non-trivial topological properties.

In summary, our results are twofold. On the one hand, we provide an efficient algorithm for pairwise state tomography with very slow scaling, which could be used even in systems many orders of magnitude larger than currently available devices. On the other hand, we propose a multiplex representation of quantum states that lends itself to a holistic statistical description of the properties of large complex quantum states. With respect to this last point, it is worth stressing that this is a very innovative and promising approach; while there has been very little work along these lines, it has already revealed that even very well-known many-body states, like the ground state of the quantum Ising model, exhibit topological properties at the complex network level that are not fully understood [87]. Our work not only widens this complex network representation by the use of a multiplex, but it also opens the path to the *experimental* reconstruction of these networks.

5.1 The algorithm

In this section we shall present the technical details of the pairwise tomography algorithm and discuss its efficiency in terms of number of required measurements.

The tomographic reconstruction of the quantum state of two qubits i

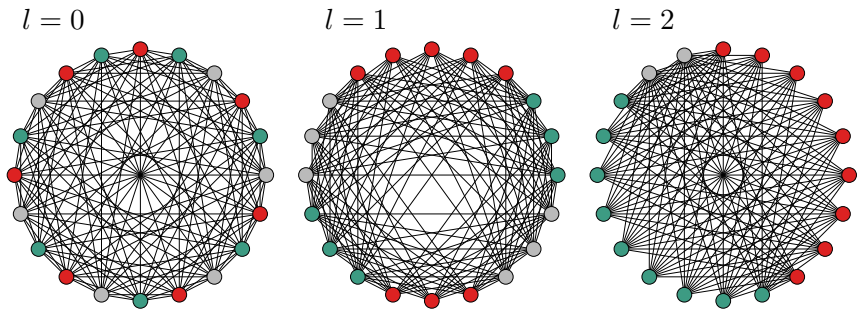

Figure 5.1: Illustration of the measurement scheme. Each figure depicts the letter assignment to each qubit (represented by three different colours) in each of the three measurement settings required for $N = 20$. The connections represent the pairs of qubits for which the relevant observables are measured. Notice that the colours are assigned according to the result of $\lfloor i/3^l \rfloor \mod 3$, where i is the qubit index (with $i = 0$ being the top-most qubit and the indices increasing in clockwise order) and $l = 0, 1, 2$ is the labelling index.

and j requires the measurement of the nine correlators of the form $\langle \sigma_a^{(i)} \otimes \sigma_b^{(j)} \rangle$, where σ_a and σ_b represent Pauli matrices with a and b taking values x, y and z. Therefore, characterising all pairwise density matrices in a system of N qubits involves measuring the average values of $9N(N-1)/2$ operators. A simple parallelization scheme, in which one measures all non-overlapping pairs of qubits at once, can reduce the number of measurement settings by a factor $\lfloor N/2 \rfloor$, thus bringing the number of required measurement setups to $\mathcal{O}(N)$.

In this section, we describe a measurement scheme, developed in paper (IV) that allows us to obtain all these observables using only $\mathcal{O}(\log N)$ measurement setups. In terms of scaling, this is an exponential improvement with respect to the naïve approach. First, notice that all the correlators $\langle \sigma_a^{(i)} \otimes \sigma_a^{(j)} \rangle \, \forall i, j$ can be obtained via a single measurement setting in which all qubits are projected onto the operator chain $\sigma_a^{(i)} \otimes \sigma_a^{(i)} \otimes .. \otimes \sigma_a^{(i)}$, we call these the trivial correlators. In the following we therefore focus on the correlators $\langle \sigma_a^{(i)} \otimes \sigma_b^{(j)} \rangle \, , a \neq b$.

We assign three different labels, q_1, q_2, and q_3, to each qubit. These three labels represent measurement bases $\sigma_x^{(i)}, \sigma_y^{(i)}$ and $\sigma_z^{(i)}$ for each qubit, in such a way that for any pair of different labels (q_i, q_j), with $i \neq j$, we

measure in two different directions, x, y, or z. By letting these three letters run over all the six possible ordered combinations of measurement bases, we make sure that all the non-trivial correlators for any two qubits with different letters will be covered. However, for pairs of qubits with equal labels, no non-trivial correlators can be measured. Hence, our algorithm aims at finding the minimal set of qubit labelling's such that all pairs of qubits are covered and all non-trivial correlators are measured.

The general algorithm is described in paper (IV) while here we give a particular small-scale example to illustrate how the algorithm works. Figure 5.1 illustrates the different labelling's, as well as the pairs of qubits covered by each of them, for $N = 20$ qubits. We initially begin by periodically labelling every consecutive qubit with a different color. This gives us the non-trivial correlators for all qubits except those pairs having the same color. The next step of the algorithm is therefore to construct larger groups of qubits of the same color, specifically groups of 3 qubits and repeating the measurements. Note that now, most qubits which previously had the same color are now colored differently. We then obtain the non-trivial correlators again and continue with the next iteration of the algorithm, now grouping the qubits in groups of $3^2 = 9$. We repeat the steps until all of the non-trivial correlators are obtained, and in paper (IV) we prove that the total number of steps is of the order of $\log_3(N)$. The required number of different measurement settings is therefore

$$6 \lceil \log_3 N \rceil + 3, \tag{5.1}$$

that is, 6 settings per labelling plus the 3 trivial ones. This means that, for example, for around $N = 50$ qubits, the size of the state-of-the-art quantum computers available today, we need less than 30 measurement settings, as opposed to more than 400 settings needed with the naïve parallel approach.

5.2 Quantum tomography multiplex

Once all the measurements in the scheme have been performed, we can reconstruct the so-called pairwise tomography network, in which every pair of qubits is assigned its corresponding reduced density operator reconstructed from the tomographic data. This network can then be unfolded into a *quantum tomography multiplex* [21, 92–95], a multilayer network involving the qubits as nodes in which, in every layer, edges represent a different pairwise

quantity.

In this work, we focus on six such quantities, namely mutual information [18], classical correlations [20], quantum discord [19], entanglement (measured via concurrence [17]), von Neumann entropy [91], and purity; to assign an edge between two qubits i and j in any of those layers, we simply compute the corresponding quantity from their reduced density matrix. In the following we define these quantities and introduce their physical meaning.

5.2.1 Quantum mutual information and von Neumann entropy

The quantum mutual information is a measure of correlation (both quantum and classical) between subsystems of quantum states. It generalizes the classical concept of mutual information to quantum systems. While the classical mutual information uses classical probability distributions and Shannon entropy, the quantum counterpart is calculated using density matrices and von Neumann entropy.

For bipartite quantum systems with Hilbert space $H_{AB} := H_A \otimes H_B$, we indicate with ρ_{AB} a density matrix of the combined system. The von Neumann entropy of a density matrix ρ_{AB} gives the information content of a density matrix in the form

$$S(\rho_{AB}) = -\operatorname{Tr} \rho_{AB} \log \rho_{AB}. \tag{5.2}$$

The von Neumann entropy of the reduced state $\rho_{B(A)}$ is $S(\operatorname{Tr}_{A(B)}[\rho_{AB}])$. The quantum mutual information is now defined as

$$I(\rho_{AB}) := S(\rho_A) + S(\rho_B) - S(\rho_{AB}). \tag{5.3}$$

This quantity is always non-negative $I(\Phi(\rho_{AB})) \geq 0$ and contractive under CPTP maps Φ:

$$I(\Phi(\rho_{AB})) \leq I(\rho_{AB}) \tag{5.4}$$

This indicates that environment-induced decoherence always reduces quantum mutual information.

5.2.2 Quantum discord and classical correlations

Quantum discord is a measure of quantum correlations more general than entanglement. In particular it reduces to entanglement for pure states, while for mixed states it can be present in absence of entanglement. It was introduced in 2001 simultaneously by L. Henderson and V. Vedral [96], and H. Ollivier and W. H. Zurek [19] as the difference between two classically equivalent definitions of mutual information, $I(\rho)$ and $J_A(\rho)$. The mathematical definition of discord on subsystem A is

$$\begin{aligned} \mathcal{D}_A(\rho_{AB}) &= I(\rho_{AB}) - \max_{\{P_j^B\}} J_{\{P_j^B\}}(\rho_{AB}), \\ J_{\rho_A}(\rho_{AB}) &= S(\rho_B) - S(\rho_B|\rho_A), \end{aligned} \tag{5.5}$$

where $S(\rho_B|\rho_A)$ is the quantum analog of conditional entropy. To understand the meaning of the second definition of mutual information $J_A(\rho)$, we need to recall that in general, any measurement on subsystem $B(A)$ affects our knowledge of the subsystem $A(B)$, unless they are completely uncorrelated. Specifically, the amount of modification of subsystem A will depend on the choice of measurement performed on B. Here we limit our attention to von Neumann measurements performed on B described by a complete set of orthonormal projectors P_j^B corresponding to a measurement outcome j. The quantum state of the total system conditioned by the measurement outcome labeled by j is the conditional density operator $\rho_j = (I^A \otimes P_j^B)\rho_{AB}(I^A \otimes P_j^B)/p_j$ where $p_j = \mathrm{Tr}[(I^A \otimes P_j^B)\rho_{AB}(I^A \otimes P_j^B)]$, I^A being the identity operator on subsystem A. The quantum analog of conditional entropy is then defined as

$$S(\rho_B|\rho_A) = \sum_j p_j S(\rho_j) \tag{5.6}$$

It can be shown that the maximum of $J_A(\rho_{AB})$ over all the possible sets of measurements can be interpreted as a measure of classical correlations of the state

$$\mathcal{C}(\rho_{AB}) = \max_{\{P_j^B\}} J_{\{P_j^B\}}(\rho_{AB}) \tag{5.7}$$

By looking at equation (5.5), we observe that the quantum discord is just the difference of quantum mutual information and classical correlations.

We see that quantum discord is an argument-wise non-symmetric quantity that depends on the choice of the measured qubit, in this thesis and in paper (IV) we show the values obtained by performing the measurement on the qubit with the smallest index.

5.2.3 Concurrence and purity

Concurrence is a measure of entanglement defined in Eq. (4.1).

Finally, purity measures the deviation of the density matrix from a pure state and is defined as

$$\gamma_P = \mathrm{Tr}[\rho^2]. \tag{5.8}$$

For pure states, $\gamma_P = 1$ and for mixed states $\gamma_P < 1$. Purity of a combined state of two qubits in a many-qubit state measures how strongly the qubit pair is entangled with the rest of the qubits.

5.3 Decoherence in complex network representations

The pairwise tomography network can be used to generate multiplex representations of quantum states, in which the connections among qubits represent different quantifiers in every layer. This can be useful, for instance, for understanding the presence of correlations, quantum or classical, between an open quantum system and its quantum environment, as well as among the different parts of the latter. Indeed, it is particularly interesting to understand whether an open system becomes entangled with the environment and to describe microscopically the presence of quantum correlations also within the environment.

The emergence of the classical world is one of the most fundamental open problems in quantum theory, with entanglement-induced decoherence standing as a cornerstone of our current knowledge on the subject. Indeed, it is commonly accepted that a quantum system loses its coherence as a result of the entanglement with its environment, which appears as a consequence of the unavoidable interactions with the latter. Interestingly it has been shown that a system interacting with a quantum environment can decohere without system-environment entanglement [97]. This can be

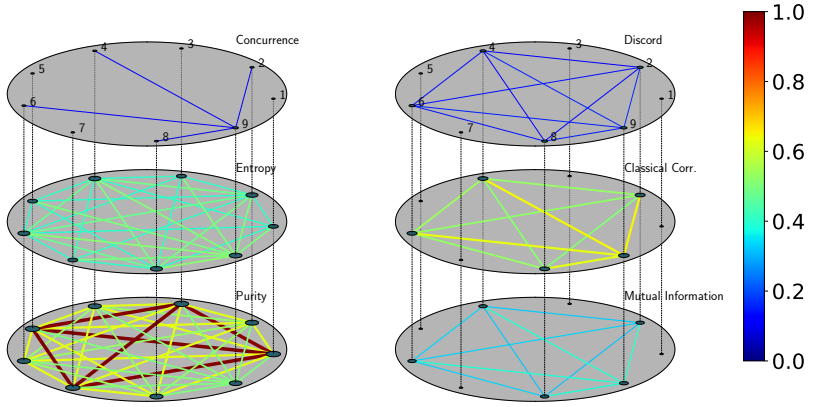

Figure 5.2: Collisional model at time $\lambda t = 1000$, and with entangling interaction strength $\theta = 2\pi/3$. Qubits 1, 3, 5, and 7 are the emitters, 2, 4, 6, and 8, the ancillae, whereas 9 is the system qubit. The concurrence reveals pairwise entanglement between the system and the ancillae only, whereas there are quantum discord, classical correlations and mutual information among the ancillae as well. The emitters are in the ground state, since they are not correlated with any other qubit, while they form a clique in the purity layer; similarly, notice that there are no connections among emitters in he entropy layer.

proven by using an exactly solvable collisional model, in which a qubit system collides with uncorrelated ancillae following a Poisson process (that is, collision times are not deterministic).

In order to illustrate this, we apply our machinery to the simulation of such a model. In particular, we assume that each ancilla collides only once at a time exponentially distributed with rate λ/n, where n is the number of ancillae. We also assume that the interaction between the system and an ancilla, driven by the Hamiltonian $H_I = \frac{\eta}{2}\sigma_x^a \otimes \sigma_z^s$, can be considered instantaneous, resulting in the unitary transformation $U_\theta = e^{-i\frac{\theta}{2}\sigma_x^a \otimes \sigma_z^s}$, where $\theta = \lim_{t\to 0} t\eta$ denotes the interaction strength and t is the duration of the collision. Furthermore, we will consider the states of the system and an ancilla to be $|+\rangle_s$ and $|0\rangle_a$, respectively, before the collision.

To illustrate the potential of the multiplex representation, we will consider here entangling interactions, as they lead to more complex quantum states and dynamics. We further give a quantum origin to the randomness in the collision times through the introduction of n emitters, initially in

the excited state, which relax to their ground state emitting an ancilla that immediately collides with the system qubit.

We have created a video showing the time evolution of the multiplex, namely, how pairwise entanglement, quantum and classical correlations, and entropy/purity are dynamically established within the system-environment framework [1]. Moreover, in Fig. 5.2, we show the multiplex of the corresponding state for $N = 9$ (that is, with 4 emitter-ancilla pairs) in the long time limit and with entangling interaction strength $\theta = 2\pi/3$. The resulting multiplex network exhibits a complex structure from which it is easy to identify the role of every qubit, i.e. system (qubit 9), emitters (qubits 1,3,5,7), or ancilla (qubits 2,4,6,8), in the dynamics. The concurrence layer reveals that the system qubit is indeed entangled with all the ancillae but not with the emitters. Interestingly, despite the lack of entanglement between the different ancillae, these are nevertheless correlated, both at the classical and at the quantum levels, with non-zero classical correlations and discord (and, consequently, mutual information). Finally, the connectivity of the emitters reveals that, as expected at long times, they are in the ground state. This is consistent with the total lack of correlations with any other qubits and with the fact that the four emitters form a strongly connected subset in the purity layer; also, their connections are even deemed statistically irrelevant in the entropy layer.

[1] See the Supplemental Material at
https://journals.aps.org/prresearch/abstract/10.1103/PhysRevResearch.2.023393

Chapter 6

Emergent entanglement structures in complex quantum networks

In this chapter, we tackle the fundamental issue of emergence of entanglement properties in many-body quantum systems through a complex networks approach. We use our experimentally accessible complex network representation for quantum many-body states. We build networks of pairwise concurrence for the ground states of the XX model, one of the most widely studied spin chain systems whose analytical solution has been known for 60 years. We use tools of complex network theory to analyse this system and in this way we reveal new physical phenomena. We unveil a new symmetry in the entanglement structure of the ground state close to the critical point. We show that the onset of long-range order is accompanied by topological instabilities in the network structure. Moreover, we find that these quantum states present emergent entanglement structures that manifest themselves as communities in the network representation. We also observe that the dependence of the structure of the state exhibits a cyclic self-similarity that results in different structural classes for a fixed magnetic field.

In summary, in this chapter we summarize the results of paper (V) and show that quantum many-body systems can present emergent phenomena, similarly to classical complex systems. Strikingly, these phenomena have gone unnoticed for the XX model that we consider in the paper. We believe the reason to be that these properties can only be unveiled when taking a holistic perspective in their analysis. Therefore we believe that the appli-

cation of mathematical tools developed for the study of classical complex systems, such as complex network theory, will result in a paradigm shift in the study of many-body physics. Our work presents a first example of the power of a comprehensive description of a quantum state from the complex systems perspective, hence setting a cornerstone in the development of this novel approach.

6.1 The XX model

We consider in the following the XX model, one of the most studied prototypical condensed matter systems, defined as a chain of N spins with nearest-neighbours interactions as follows:

$$H = -J \sum_{i=1}^{N} \left[\frac{1}{2} (\sigma_x^i \sigma_x^{i+1} + \sigma_y^i \sigma_y^{i+1}) + B \sigma_z^i \right], \tag{6.1}$$

with J the coupling constant, which hereafter we set to unity, and B the magnetic field. In the thermodynamic limit, the ground state of this system undergoes a first order quantum phase transition from a fully polarized state to a critical phase exhibiting quasi-long-range order for $B = 1$ [98–100]. The model can be solved exactly by means of Jordan-Wigner transformations [101].

Specifically, one defines the operators

$$d_k = \sqrt{\frac{2}{N+1}} \sum_{l=1}^{N} \sin\left(\frac{\pi k l}{N+1}\right) \bigotimes_{m=1}^{l-1} \sigma_z^m \sigma_-^l, \tag{6.2}$$

which transform the Hamiltonian of Eq. (6.1) as follows

$$H = \sum_{k=1}^{N} \Lambda_k d_k^\dagger d_k + NB\mathbf{I} \tag{6.3}$$

with eigenvalues $E_i = \sum_{k=1}^{N} \Lambda_k \alpha_k^i + NB$, with $\Lambda_k = -2B + 2\cos[(\pi k)/(N+1)]$, where $\alpha_k^i = \langle \psi_i | d_k^\dagger d_k | \psi_i \rangle$ takes values $0, 1$ and $|\psi_i\rangle$ is the corresponding eigenvector.

The structure of the ground state and its energy vary with the magnetic field B and, specifically, they depend on a number of level crossings in terms

of distinct ground states that the system undergoes as B changes. It has been shown that, for $B > 1$, the ground state energy is $\epsilon_g^0 = -NB$ and the ground state is $|\phi_g^0\rangle = |\uparrow\rangle^{\otimes N}$, which is separable [99]. For $0 < B < 1$, we can identify k level crossings for values of the magnetic field given by $B_k = \cos[k\pi/(N+1)]$, with $1 \leq k \leq N$. In each region defined by $B_{k+1} < B < B_k$, the ground state energy is

$$\epsilon_g^k = -(N-2k)B - 2\sum_{l=1}^{k} \cos\left(\frac{\pi l}{N+1}\right) \tag{6.4}$$

and the ground state is given by

$$|\phi_g^k\rangle = \sum_{l_1<l_2<\ldots<l_k} A_{l_1 l_2 \ldots l_k} |l_1, l_2, ..., l_k\rangle, \tag{6.5}$$

with $|l_1, l_2, ..., l_k\rangle$ the state with flipped spins at sites $l_1, l_2, ..., l_k$, and amplitudes given by

$$A_{l_1 l_2 \ldots l_k} = \sum_P (-1)^P S_{l_1}^{P(1)} S_{l_2}^{P(2)} \ldots S_{l_k}^{P(k)},$$

where the sum extends over the permutation group and where

$$S_l^k = \sqrt{2/(N+1)} \sin[(\pi k l)/(N+1)]. \tag{6.6}$$

At $B = B_k$, the ground state jumps discontinuously from one symmetric subspace to an orthogonal one.

The properties of pairwise concurrence for the XX model were studied in Ref. [99], where it was shown that an analytical expression for the pairwise concurrence can be straightforwardly obtained from the reduced two-spin density operators and reads as follows

$$C_{l,m} = 2\max\left\{0, |e| - \sqrt{a_+ a_-}\right\}, \tag{6.7}$$

where

$$\begin{aligned} e &= \tfrac{1}{2}\langle \sigma_l^x \sigma_m^x \rangle, \\ a_\pm &= \tfrac{1}{4}[1 \pm \langle \sigma_l^z \rangle \pm \langle \sigma_m^z \rangle + \langle \sigma_l^z \sigma_m^z \rangle]. \end{aligned} \tag{6.8}$$

The transversal and longitudinal two-points correlation functions $\langle \sigma_l^z \sigma_m^z \rangle$

and $\langle \sigma_l^x \sigma_m^x \rangle$ respectively, can be efficiently measured with the pairwise tomography approach that we descried in the previous chapter. Their analytical expressions given in Ref. [99] are used to show that pairwise entanglement presents discontinuous jumps at the transition points B_k, and moreover entanglement between two spins in the bulk and at the edge of the chain shows very different behaviour signalling the onset of quasi-long range order. These results only concern the thermodynamic limit, where concurrence only depends on the distance between spins. Our powerful network representation, however, allows us to go beyond the thermodynamic limit results and study finite size effects.

We stress that in the literature of quantum spin Hamiltonians, and generally when studying quantum phase transitions, one often works in the thermodynamic limit or considers closed boundary conditions wherein translational invariance is generally guaranteed. This implies that most two-spin correlation functions, including concurrence which is built on them, depend only on the distance between the spins [100, 102, 103]. However, for realistic experimental scenarios, i.e., for quantum simulators, the quantum systems are neither close to the thermodynamic limit nor have closed boundary conditions. Therefore, the analysis of the full network of pairwise correlations becomes essential.

6.2 Network of pairwise concurrence

In Figure 6.1 we illustrate concurrence networks for different values of k or equivalently, of the magnetic field. We see that, as we change the magnetic field, the topology of the concurrence network changes abruptly across the transition points B_k. In order to gain more information on the properties of each of the k ground states, we use a toolbox from complex network theory.

We start our analysis of the weighted structure of the state by making use of two local measures: strength and disparity, which we depict for each spin in the chain in Fig. 6.2**a-b**. We can see from this figure that, close to the critical point $B = 1$ ($k = 0$), the local (single-spin) distribution of concurrences is very homogeneous as indicated by the fact that the disparity is essentially constant along the chain. At the same time, the strength curve reveals that pairwise entanglement is much stronger for central spins than for those at the ends of the chain. This means, together with the fact

that the graph is fully connected (all degrees are equal to $N-1$), that concurrences are actually heterogeneously distributed across the system. Yet, these weights are allocated in such a way that all relative fluctuations at the local level, quantified by the disparity, are equal. This indicates a high level of symmetry in the state right before the quantum phase transition, namely, that the single-spin distributions of concurrence may be very similar for all spins in the chain when appropriately rescaled; this is indeed confirmed in Fig. 6.2**d**.

As the magnetic field is decreased (and k increases), we observe the appearance of $k-1$ maxima in the disparity, signalling a local increase in the heterogeneity of pairwise concurrence for centrally located spins. A close inspection of the plots also shows that the outermost (and highest) peaks in Y_i correspond to the outermost (and lowest) minima in the strength s_i, which presents k peaks. In short, we see that there are field-dependent groups of spins near the boundaries exhibiting higher, and more homogeneously distributed, pairwise entanglement, which we may consider as *edges*. The rest of the spins in the chain, with lower and more heterogeneous local concurrence distribution, will be denoted as the *bulk* of the chain. Moreover, these regions are very clearly delimited and their size strongly depends on the magnetic field, for fixed N.

Interestingly, as the magnetic field decreases, the difference between the disparity of the bulk of the chain and the one of the edge decreases until, for $B = 1/2$ ($k/(N+1) = 1/3$) their respective values get inverted, namely the bulk disparity becomes lower than the edge disparity. For very small values of B one observes a pronounced disparity peak for the two outermost spins of the chain, corresponding to their highest value of pairwise concurrence; this phenomenon is a reflection of the fact that, for small B, the network has a nearest-neighbour chain topology, as a result of which the edge spins have degree equal to one, and hence their disparity can only be equal to one, see also Fig. 6.1. Additional insight into the properties of the state can be obtained by investigating the average behaviour of the network measures which is also sensitive to the critical points. We consider the average disparity $\langle Y_i \rangle$ and the average strength $\langle s_i \rangle$ in Fig. 6.2**c** showing that the discontinuous jumps present for small N gradually become less visible as we approach the thermodynamic limit. The average strength changes discontinuously at the critical point $B = 1$, while the average disparity, measuring entanglement heterogeneity, is undefined for $B > 1$, since concurrence is zero for all pairs.

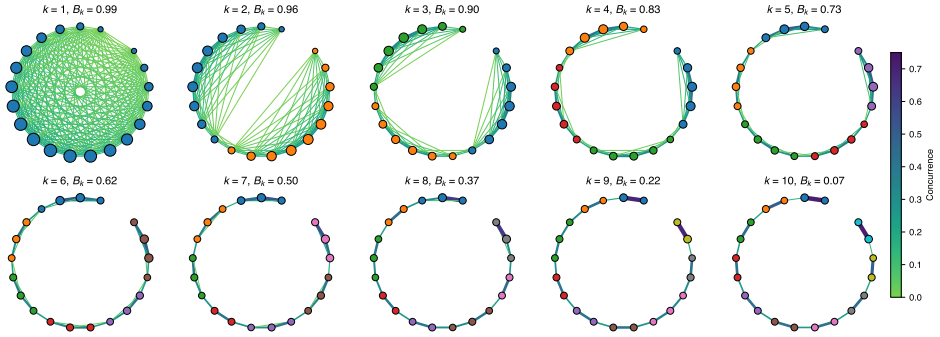

Figure 6.1: Concurrence networks for $N = 20$ spins for different values of the magnetic field B_k for $k = 1, 2, \ldots, 10$. Each node represents a different spin. The width and colour of the links indicate the value of the concurrence between the corresponding pair, while the sizes of the nodes are proportional to their strength. The colours of the nodes identify the community structure detected by the LPA algorithm. The number of communities is found to be equal to k.

6.3 Emergent entanglement structures

The network measures used in the previous section reveal local structures within the concurrence network. Networks, however, may also possess mesoscopic structures, which are not uncovered at the level of single nodes. Examples are the network community structures describing the heterogeneity in the density of links or in the values of the weights within different subsets of the nodes of the network. We call community a subset of nodes with higher density of connections within the subset than with the rest of the network. Detection of and therefore definition of communities is a non-unique algorithm-dependent process and may not reproduce exactly the same result even for a single algorithm, due to different initial random seeds. The presence of communities is linked to a non-trivial topology of the network: regular and completely random graphs typically do not show any community structure.

In paper (V) we use community detection algorithms to uncover the community structure of pairwise concurrence graph. Many such algorithms have been developed and are being developed to achieve the goal of finding the community structure of large networks quickly and accurately [104]. In this chapter, we apply a state-of-the-art algorithm, based on label propa-

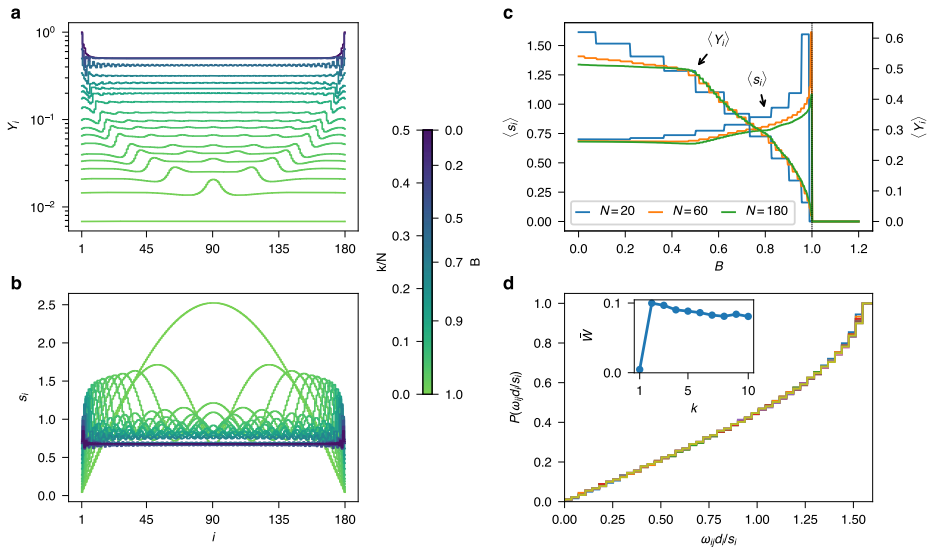

Figure 6.2: **Disparity and strength in entanglement networks.** **a**, Disparity Y_i by node for $N = 180$ and for different values of the magnetic field $0 < B < 1$. Note that the disparity has $k-1$ peaks and its average value increases with k (decreases with B). **b**, Strength s_i of each node for the same states as in **a**. The curve corresponding to the k-th state presents k maxima. The bar next to the plots indicates the values of the magnetic field B (equivalently, of k/N) to which each colour corresponds. For the sake of clarity, the plots do not include the results for all the values of k. **c**, Average strength $\langle s_i \rangle$ and average disparity $\langle Y_i \rangle$ as functions of B for different values of N (20, 60, 180). **d**, Each of the overlapping curves depicts the cumulative distribution of the concurrences of a different spin in the chain, rescaled by the average of the distribution, s_i/d_i. **Inset**, Average over all the pairs of spins in the k-th state of the Wasserstein distance W between their rescaled local weight distributions. It can be appreciated that this quantity drops to nearly zero for $k = 1$.

gation (LPA) [105], which is described in detail in paper (V).

An example of the communities detected with LPA is shown in Fig. 6.1, where nodes with the same colour belong to the same community. It is important to stress that the LPA algorithm is completely model-agnostic, in the sense that it is designed to work on arbitrary weighted graphs that may represent any sort of data. Remarkably, the entanglement structures identified by community detection method have well-defined spatial locations. For small N, the community structure is clearly visible from the

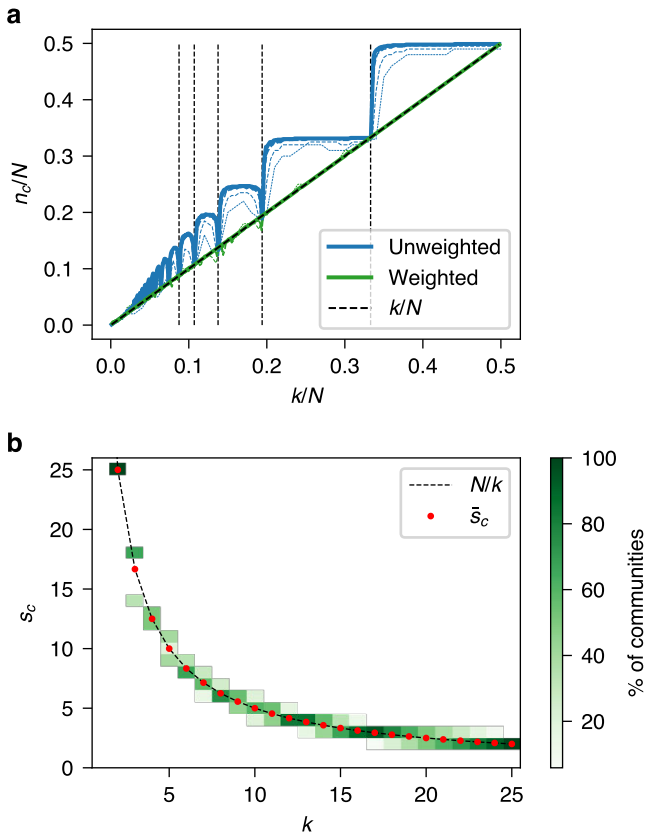

Figure 6.3: **Community structure of concurrence networks**. **a**, Number of communities in the concurrence network over N, n_c/N, as a function of k/N, for $N = 100, 200, 500, 600, 960$, by treating the edges as unweighted (blue) and weighted (green). In the weighted case, the number of detected communities is exactly equal to k (with some fluctuations due to numerical errors), regardless of N. The unweighted case is more complex and is discussed in paper (V). The colour indicates the fraction of communities with a given size. The black dashed line shows N/k, while the red points indicate the average size $\bar{s}_c$ of the detected communities. **b** Community sizes S_c versus k for $N = 50$. The colour indicates the fraction of communities with a given size. The black dashed line shows N/k, while the red points indicate the average size $\bar{s}_c$ of the detected communities.

network representation, as one can see in Fig. 6.1. For small k, there are few large communities of nodes with nonzero pairwise entanglement. By increasing k, the size of the communities is reduced, up to the limit for $k = N/2$, where all the communities have size 2, and correspond to pairs of highly entangled spins.

Strikingly, for each value of k, the algorithm detects, allowing for small numerical fluctuations, $n_c = k$ communities on the weighted networks on any N, as Fig. 6.3**a** shows. The average size of the communities is therefore $\bar{s}_c = N/k$. Moreover, the distribution of community sizes is highly peaked around the mean, as shown in Fig. 6.3**b**. We note that, for low B_k the graphs are essentially m-nearest-neighbours lattices for a wide range of k, so the difference in the community structure is much more subtle than for the top-left networks in Fig. 6.1. In fact, when applying the community detection algorithm to the unweighted concurrence networks, obtained by transforming $C_{ij} \to \Theta(C_{ij})$, the inferred community structure changes considerably, as can be seen from the blue curves in Fig. 6.3**a**. Specifically, the number of detected communities n_c versus k show plateaus where n_c is roughly constant, interrupted by dips that appear at certain values of k/N (see paper (V) for more details). Hence, we conclude that, the community structure must be encoded in the dependence of the concurrence with respect to the position along the chain.

Note that k is the quantum number associated to the total magnetisation $\sum_i \sigma_z^i$, which is a constant of motion. Hence the emergent entanglement structures described in this section reflect a global symmetry of the system.

Summarizing, we have discovered and discussed here a new emergent phenomenon in the ground state of a paradigmatic condensed matter system at criticality. We believe that this is just one example of the power of the complex network representation and of the associated toolbox borrowed from classical network theory. In the future, we plan to apply this formalism to the study of more complex spin chain models (such as the XY model) and carry forward connections between this system and relativistic systems such as Hawking radiation and black holes [23].

Conclusions and outlook

Throughout the thesis we have seen how the tools of open quantum systems and complex quantum networks can be used to discover new features in paradigmatic models in condensed matter and relativistic quantum physics. What we have attempted is to begin a larger mathematical framework which combines different methods to connect separate fields together. Metaphorically speaking, the different fields are akin to pieces of a big and fascinating puzzle whose solution would give us a coherent unified description of quantum theory and general relativity. While we are aware of the ambitiousness of this program, we think that a way to proceed is to use complex quantum networks to bridge the gap with both open quantum systems and general relativity. We would like to conclude this thesis by mentioning few potential future directions that follow naturally from our results and build on very recent scientific discoveries.

The central concept from which our future work will stem is the description of black holes and Hawking radiation. On the one hand we plan to extend the results of Chapter 3 from Unruh effect to Hawking radiation. It is well known that these are closely related phenomena and we therefore expect such a connection to be possible. On the other hand we consider the recent results obtained in Ref. [23] wherein a one-to-one correspondence between a massless Dirac field and a site-dependent XX model is discovered. This allows one to simulate Hawking radiation of a black hole by means of quantum many-body systems. Moreover, the quantum many-body system used is a generalization of the one we have studied in paper (V). Hence we plan to use the complex network representation and the tools of complex network theory to describe black holes. A further subsequent step would be to establish a connection between the complex network representation and possible emergent geometries. In Ref. [106], the authors construct a spatial manifold and its geometry from the entanglement structure of an abstract quantum state in Hilbert space. In particular, they consider the Heisenberg spin chain models (of which the XX model is a special case) and

build networks of pairwise mutual information to define a distance measure on the graph from where they obtain emergent geometry. This general result can be applied to the network representation of the black hole which we intend to pursue, therefore linking the description of curved spacetime to emergent geometry via pairwise entanglement.

Finally, we would like to benchmark this approach with the recently proposed physical picture of the notion of emergent time consistent with both classical and quantum descriptions in the large-N limit [1]. Also in this paper a theoretical framework describing black holes is developed starting from a quantum mechanical description and emergent geometry is considered. The approach of Ref. [1] relies on the so-called Page and Wootters mechanism [107], which is an attempt of a quantum mechanical description of emergent time.

In conclusion, while the research performed for the thesis followed a somewhat scattered path, passing through stages which did not initially seem connected, an overall view reveals a deep and fascinating underlying interrelation. Each step of the path, however, was educational and tremendously useful. Writing the thesis itself helped to clarify the common base and inspired exciting future directions.

Bibliography

[1] C. Foti, A. Coppo, G. Barni, A. Cuccoli, and P. Verrucchi, *There is only one time* (2020), 2006.12103.

[2] W. F. Stinespring, Proc. Amer. Math. Soc. **6**, 211 (1955), ISSN 0002-9939.

[3] A. Fujiwara and P. Algoet, Phys. Rev. A **59**, 3290 (1999).

[4] I. Pikovski, M. Zych, F. Costa, and Č. Brukner, Nature Physics **1**, 668 (2015).

[5] W. Zurek, Physics Today **44** (2003).

[6] C. T. Lee, Phys. Rev. A **44**, R2775 (1991).

[7] A. Kenfack and K. Życzkowski, Journal of Optics B: Quantum and Semiclassical Optics **6**, 396–404 (2004), ISSN 1741-3575.

[8] W. Vogel, Phys. Rev. Lett. **84**, 1849 (2000).

[9] D. Klyshko, Physics Letters A **213**, 7 (1996), ISSN 0375-9601.

[10] F. Benatti and R. Floreanini, Phys. Rev. A **70**, 012112 (2004).

[11] H.-P. Breuer, E.-M. Laine, and J. Piilo, Phys. Rev. Lett. **103**, 210401 (2009).

[12] H.-P. Breuer, E.-M. Laine, J. Piilo, and B. Vacchini, Rev. Mod. Phys. **88**, 021002 (2016).

[13] L. Li, M. J. W. Hall, and H. M. Wiseman, Phys. Rep. **759**, 1 (2018).

[14] A. Rivas, S. Huelga, and M. Plenio, Rep. Prog. Phys. **77**, 094001 (2014).

[15] C.-F. Li, G.-C. Guo, and J. Piilo, Eur. Lett. **127**, 50001 (2019).

[16] R. Saeidinia and A.-L. Barabási, *Network Science: Albert-Laszlo Barabasi* (Cambridge University Press, 2017).

[17] W. K. Wootters, Phys. Rev. Lett. **80**, 2245 (1998).

[18] B. Schumacher and M. D. Westmoreland, Phys. Rev. A **74**, 042305 (2006).

[19] H. Ollivier and W. H. Zurek, Phys. Rev. Lett. **88**, 017901 (2001).

[20] B. Groisman, S. Popescu, and A. Winter, Phys. Rev. A **72**, 032317 (2005).

[21] G. Bianconi, *Multilayer networks: structure and function* (Oxford University Press, 2018).

[22] W. Heisenberg, Zeitschrift für Physik **49**, 619 (1928), ISSN 0044-3328.

[23] R.-Q. Yang, H. Liu, S. Zhu, L. Luo, and R.-G. Cai, Phys. Rev. Research **2**, 023107 (2020).

[24] R. D. Purrington, *The heroic age, the creation of quantum mechanics, 1925–1940* (Oxford University Press, 2018).

[25] W. Heisenberg, Zeitschrift fur Physik **43**, 172 (1927).

[26] L. E. Ballentine, *States, Pure and Mixed, and Their Representations* (Springer Berlin Heidelberg, Berlin, Heidelberg, 2009), ISBN 978-3-540-70626-7.

[27] E. Schrödinger, Phys. Rev. **28**, 1049 (1926).

[28] V. Gorini, A. Kossakowski, and E. Sudarshan, J. Math. Phys. **17**, 821 (1976).

[29] G. Lindblad, Commun. Math. Phys. **48**, 119 (1976).

[30] H.-P. Breuer and F. Petruccione, *The Theory of Open Quantum Systems* (Oxford University Press (New York), 2007)).

[31] M. A. Nielsen and I. L. Chuang, Phys. Rev. Lett. **79**, 321 (1997).

[32] D. Chruściński, A. Kossakowski, and A. Rivas, Phys. Rev. A **83**, 052128 (2011).

[33] D. Chruściński, A. Rivas, and E. Størmer, Phys. Rev. Lett. **121**, 080407 (2018).

[34] B. Bylicka, M. Johansson, and A. Acin, Phys. Rev. Lett. **118**, 120501 (2017).

[35] A. Smirne, J. Kołodyński, S. F. Huelga, and R. Demkowicz-Dobrzański, Phys. Rev. Lett. **116**, 120801 (2016).

[36] H. Lyyra, Ph.D. thesis, University of Turku, Department of Physics and Astronomy (2019).

[37] L. Mazzola, S. Maniscalco, J. Piilo, K.-A. Suominen, and B. M. Garraway, Phys. Rev. A **80**, 012104 (2009).

[38] S. Weinberg, *Gravitation and Cosmology: Principles and Applications of the General Theory of Relativity* (John Wiley & Sons, Inc., 1972).

[39] A. Einstein, Ann. Physik **17**, 891 (1905).

[40] A. Einstein, Ann. Physik **18**, 639 (1905).

[41] R. V. Pound and G. A. Rebka, Phys. Rev. Lett. **3**, 439 (1959).

[42] T. Nicholson, S. Campbell, R. Hutson, G. Marti, B. Bloom, R. McNally, W. Zhang, M. Barrett, M. Safronova, G. Strouse, et al., Nat Commun. **6**, 6896 (2015).

[43] I. Pikovski, M. Zych, F. Costa, and Č. Brukner, New Journal of Physics **19**, 025011 (2017).

[44] D. Chruściński and S. Maniscalco, Phys. Rev. Lett. **112**, 120404 (2014).

[45] J. Paavola and S. Maniscalco, Phys. Rev. A **82**, 012114 (2010).

[46] J. Paavola, M. J. W. Hall, M. G. A. Paris, and S. Maniscalco, Phys. Rev. A **84**, 012121 (2011).

[47] S. Maniscalco, J. Piilo, F. Intravaia, F. Petruccione, and A. Messina, Phys. Rev. A **70**, 032113 (2004).

[48] Maniscalco, S., Piilo, J., and Suominen, K.-A., Eur. Phys. J. D **55**, 181 (2009).

[49] V. Dodonov, I. Malkin, and V. Man'ko, Physica **72**, 597 (1974), ISSN 0031-8914.

[50] F. Steiner, Physica B+C **151**, 323 (1988), ISSN 0378-4363.

[51] J. P. Paz, S. Habib, and W. H. Zurek, Phys. Rev. D **47**, 488 (1993).

[52] J. Trapani, M. Bina, S. Maniscalco, and M. G. A. Paris, Phys. Rev. A **91**, 022113 (2015).

[53] G. M. D'Ariano, M. F. Sacchi, and P. Kumar, Phys. Rev. A **59**, 826 (1999).

[54] M. Carlesso and A. Bassi, Physics Letters A **380**, 2354 (2016), ISSN 0375-9601.

[55] C. Monroe, D. M. Meekhof, B. E. King, and D. J. Wineland, Science **272**, 1131 (1996), ISSN 0036-8075.

[56] W. G. Unruh, Phys. Rev. D **14**, 870 (1976).

[57] L. C. B. Crispino, A. Higuchi, and G. E. A. Matsas, Rev. Mod. Phys. **80**, 787 (2008).

[58] V. Mukhanov and S. Winitzki, *Introduction to quantum effects in gravity* (Cambridge University Press, 2013).

[59] N. D. Birrell and P. C. W. Davies, *Quantum fields in curved space* (Cambridge Univ. Press, 1982).

[60] W. Unruh and R. Wald, Phys. Rev. D **29**, 1047 (1984).

[61] J. Louko and A. Satz, Class. Quant. Grav. **23**, 6321 (2006).

[62] J. Nokkala, Ph.D. thesis, University of Turku, Department of Physics and Astronomy (2018).

[63] J. Nokkala, F. Galve, R. Zambrini, S. Maniscalco, and J. Piilo, Sci. Rep. **6**, 26861 (2016), ISSN 2045-2322.

[64] T. H. Johnson, S. R. Clark, and D. Jaksch, EPJ Quantum Technology **1**, 10 (2014).

[65] J. Zhang, G. Pagano, P. W. Hess, A. Kyprianidis, P. Becker, H. Kaplan, A. V. Gorshkov, Z.-X. Gong, and C. Monroe, Nature **551**, 601 (2017).

[66] H. Bernien, S. Schwartz, A. Keesling, H. Levine, A. Omran, H. Pichler, S. Choi, A. S. Zibrov, M. Endres, M. Greiner, et al., Nature **551**, 579 (2017).

[67] S. Lloyd, Science **273**, 1073 (1996).

[68] J. Berges, Nature **569**, 339 (2019).

[69] A. Smith, M. S. Kim, F. Pollmann, and J. Knolle, npj Quantum Inf. **5**, 106 (2019).

[70] S. Montangero, *Introduction to Tensor Network Methods* (Springer International Publishing, 2018).

[71] K. Banaszek, M. Cramer, and D. Gross, New J. Phys. **15**, 125020 (2013).

[72] J. Eisert, D. Hangleiter, N. Walk, I. Roth, D. Markham, R. Parekh, U. Chabaud, and E. Kashefi, Nat. Rev. Phys. p. 382–390 (2020).

[73] J. Biamonte, M. Faccin, and M. D. Domenico, Commun. Phys. **2**, 53 (2019).

[74] A. Acín, J. I. Cirac, and M. Lewenstein, Nature Physics **3**, 256 (2007).

[75] M. Cuquet and J. Calsamiglia, Phys. Rev. Lett. **103**, 240503 (2009).

[76] S. Perseguers, M. Lewenstein, A. Acín, and J. I. Cirac, Nature Physics **6**, 539 (2010).

[77] M. Faccin, T. Johnson, J. Biamonte, S. Kais, and P. Migdał, Phys. Rev. X **3**, 041007 (2013), ISSN 2160-3308.

[78] G. D. Paparo and M. A. Martin-Delgado, Sci. Rep. **2**, 444 (2012).

[79] E. Sánchez-Burillo, J. Duch, J. Gómez-Gardeñes, and D. Zueco, Sci. Rep. **2**, 605 (2012).

[80] M. Faccin, P. Migdal, T. H. Johnson, V. Bergholm, and J. D. Biamonte, Phys. Rev. X **4**, 1 (2014), ISSN 21603308.

[81] S. Chakraborty, L. Novo, A. Ambainis, and Y. Omar, Phys. Rev. Lett. **116**, 100501 (2016), URL `https://link.aps.org/doi/10.1103/PhysRevLett.116.100501`.

[82] O. Mülken, M. Dolgushev, and M. Galiceanu, Phys. Rev. E **93**, 022304 (2016).

[83] A. Cabot, F. Galve, V. M. Eguíluz, K. Klemm, S. Maniscalco, and R. Zambrini, npj Quantum Inf. **4**, 57 (2018).

[84] J. Nokkala, F. Arzani, F. Galve, R. Zambrini, S. Maniscalco, J. Piilo, N. Treps, and V. Parigi, New J. Phys. **20**, 053024 (2018), ISSN 1367-2630.

[85] J. Nokkala, S. Maniscalco, and J. Piilo, Sci. Rep. **8**, 13010 (2018), ISSN 2045-2322.

[86] M. A. Valdez, D. Jaschke, D. L. Vargas, and L. D. Carr, Phys. Rev. Lett. **119**, 225301 (2017).

[87] B. Sundar, M. A. Valdez, L. D. Carr, and K. R. A. Hazzard, Phys. Rev. A **97**, 052320 (2018).

[88] G. De Chiara and A. Sanpera, Rep. Prog. Phys. **81**, 074002 (2018), ISSN 0034-4885.

[89] R. Albert and A.-L. Barabási, Rev. Mod. Phys. **74**, 47 (2002).

[90] M. Paris, *Quantum state estimation* (Springer-Verlag Berlin and Heidelberg Gmbh & Co. Kg, 2010).

[91] J. von Neumann, *Mathematical Foundations of Quantum Mechanics* (Princeton University Press, 1955).

[92] M. De Domenico, A. Solé-Ribalta, E. Cozzo, M. Kivelä, Y. Moreno, M. A. Porter, S. Gómez, and A. Arenas, Phys. Rev. X **3**, 041022 (2013).

[93] M. Kivelä, A. Arenas, M. Barthelemy, J. P. Gleeson, Y. Moreno, and M. A. Porter, Journal of Complex Networks **2**, 203 (2014), ISSN 2051-1310.

[94] M. De Domenico, V. Nicosia, A. Arenas, and V. Latora, Nat. Commun. **6**, 6864 (2015), ISSN 2041-1723.

[95] E. Cozzo, G. F. d. Arruda, F. A. Rodrigues, and Y. Moreno, *Multiplex networks: basic formalism and structural properties* (Springer, 2018).

[96] L. Henderson and V. Vedral, Journal of Physics A: Mathematical and General **34**, 6899 (2001).

[97] G. García-Pérez, D. A. Chisholm, M. A. C. Rossi, G. M. Palma, and S. Maniscalco, Phys. Rev. Research **2**, 012061 (2020).

[98] L. Amico, R. Fazio, A. Osterloh, and V. Vedral, Rev. Mod. Phys. **80**, 517 (2008).

[99] W. Son, L. Amico, F. Plastina, and V. Vedral, Phys. Rev. A **79**, 1 (2009), ISSN 10502947.

[100] T. J. Osborne and M. A. Nielsen, Phys. Rev. A **66**, 032110 (2002), ISSN 1050-2947.

[101] E. Lieb, T. Schultz, and D. Mattis, Annals of Physics **16**, 407 (1961), ISSN 0003-4916.

[102] A. Osterloh, L. Amico, G. Falci, and R. Fazio, Nature **416**, 608 (2002), ISSN 0028-0836.

[103] L. Amico, R. Fazio, A. Osterloh, and V. Vedral, Rev. Mod. Phys. **80**, 517 (2008).

[104] S. Fortunato and D. Hric, Physics Reports **659**, 1 (2016), ISSN 0370-1573, community detection in networks: A user guide.

[105] U. N. Raghavan, R. Albert, and S. Kumara, Phys. Rev. E **76**, 036106 (2007).

[106] C. Cao, S. M. Carroll, and S. Michalakis, Phys. Rev. D **95**, 024031 (2017).

[107] D. N. Page and W. K. Wootters, Phys. Rev. D **27**, 2885 (1983).

UNIVERSITY OF TURKU

Painosalama Oy, Turku, Finland 2020

ISBN 978-951-29-8235-6 (PRINT)
ISBN 978-951-29-8236-3 (PDF)
ISSN 0082-7002 (Print)
ISSN 2343-3175 (Online)